ISO 834 standard fire test and mechanism analysis of square tubed-reinforced-concrete columns

Dongdong Yang [a,b], Faqi Liu [a,b,*], Shan-Shan Huang [c], Hua Yang [a,b]

[a] *Key Lab of Structures Dynamic Behaviour and Control (Harbin Institute of Technology), Ministry of Education, Heilongjiang, Harbin 150090, China*

[b] *Key Lab of Smart Prevention and Mitigation of Civil Engineering Disasters (Harbin Institute of Technology), Ministry of Industry and Information Technology, Heilongjiang, Harbin 150090, China*

[c] *Department of Civil and Structural Engineering, The University of Sheffield, Sir Frederick Mappin Building, Mappin Street, Sheffield S1 3JD, UK*

Abstract

The tubed-reinforced-concrete (TRC) column is an innovative steel-concrete composite column and its steel tube is terminated at beam-to-column connections to mainly work as hoop reinforcements without sustaining axial load directly. Fire performance of TRC columns differs from that of concrete-filled steel tubular (CFST) columns since the axial deformation behaviour of the TRC columns would mainly depend on the inner reinforced concrete and local buckling of steel tube is minimised. However, no research has been reported on the behaviour of square TRC columns under fire exposure. Five slender square TRC columns subjected to standard fire and axial loading were tested in this study and the effects of load ratio and load eccentricity were investigated. Failure mode of the test specimens was dominated by global flexural buckling, whereas tube local buckling was also observed. The experimental results show that load ratio has a significant influence on the fire resistance of test specimens while the influence of load eccentricity is marginal. A sequentially-coupled thermo-mechanical finite element analysis (FEA) model was developed using ABAQUS. This FEA model was validated well against the test results when using the measured column end rotations as realistic boundary conditions. Different from the case of a CFST column, the axial load applied to a TRC column in fire is mainly sustained by the concrete and reinforcing bars and the high-temperature capacity contribution of steel tube is neglectable. With the increase of exposure time, the applied load gradually transfers from concrete to reinforcements until the

yielding of re-bars.

Keywords: Square tubed-reinforced-concrete (TRC) column; Composite construction; Fire; Experiment; FEA modelling.

* Corresponding author, E-mail address: fqliu@hit.edu.cn (F. Liu)

1. Introduction

Tubed-reinforced-concrete (TRC) column, also known as steel tube confined reinforced concrete (STCRC) column, as shown in Fig. 1, is an innovative steel-concrete composite column, which differs from conventional concrete-filled steel tubular (CFST) column, even though their appearances are similar [1-2]. The outer steel tube in TRC columns is discontinued at the beam-to-column connections and the steel tube does not directly bear axial load and mainly works as hoop reinforcements to provide confinement to the concrete core, which means local buckling of steel tube can be effectively prevented or delayed. The steel tubes used in TRC columns are generally much thinner than those used for CFST columns; the steel tube to concrete area ratio is generally between 2%-4% for TRC columns. Unlike CFST columns, which usually do not need longitudinal re-bars if fire resistance design is not required [3], longitudinal re-bars are essential to TRC columns to resist bending moments due to the discontinuity of steel tube.

The concept of TRC columns was first proposed by Tommi et al. [4-6] to improve the shear capacity and ductility of reinforced concrete (RC) columns. Aboutaha and Machado [7] also considered this member as a retrofitting method to enhance the seismic performance of RC columns. In China, TRC columns are studied as a new type of composite column and their compressive behaviour and seismic performance have been investigated by many Chinese researchers, e.g. the works conducted by Han et al. [8-9], Zhang and Liu [10], Liu et al. [11], Yu et al. [12], Abdullah et al. [13], Zhou and Liu [14] and Wang et al. [15]. TRC columns were found to possess the advantages of CFST columns, i.e. high load-bearing capacity, good ductility, excellent seismic performance and ease of construction. Furthermore, the RC beam-TRC column connections could be designed and constructed following the provisions of RC structures [1-2], as shown in Fig. 1, which avoids the complexity of connecting RC beams to CFST columns. In recent years, TRC columns are gaining increasing usage in high-rise buildings and large-span stadiums in China [15-16]. The details of the applications of TRC columns in typical engineering projects in China are listed in Table 1. This novel type of composite column is expected to have broad application prospects worldwide.

Recent fire incidents such as those of the London Grenfell Tower, Dubai Torch Tower, Melbourne Lacrosse Building and Beijing CCTV Headquarters have drawn increasing attentions to the fire engineering design of high-rise buildings [17]. However, the understanding of the fire performance of TRC columns is still very limited by far. Over the past few decades, extensive studies have been conducted on the fire behaviour of CFST columns both experimentally and numerically, e.g. the works of Han [18], Lie and Kodur [19], Wang [20], Hong and Varma [21], Romero et al. [22], Tao et al. [23], Yang et al. [24], Pagoulatou et al. [25], Meng et al. [26-27], Huang and Burgess [28], Yu et al. [29] and Yang et al. [30]. Considerable research has also been carried out to investigate the fire performance of RC columns, e.g. the works of Klingsch et al. [31], Lie and Woollerton [32], Vandevelde et al. [33], Kodur et al. [34], Tan and Yao [35], Bratina et al. [36], Wu et al. [37], Sadaoui and Khennane [38], Martins and Rodrigues [39], Bamonte and Monte [40] and Achenbach and Morgenthal [41].

However, when exposed to fire, TRC columns behave very differently compared to CFST columns and RC columns. Therefore, the outcomes of the research on the fire performance of CFST and RC columns are not directly applicable to TRC columns. There are two main differences between the fire behaviour of TRC columns and CFST columns:

(1) The axial expansion or contraction of a TRC column in fire mainly depends on the inner RC section, whereas the axial deformation of a CFST column in fire is highly affected by the steel tube. Therefore, the axial load redistributions throughout heating within the composite sections and the restraints from surrounding structures onto the heated columns are very different for these two types of columns;

(2) The steel tube of a CFST column sustains the axial load directly and is prone to local buckling. In fire conditions, the steel tube expands more than the concrete core and its axial stress increases significantly, leading to a much higher risk of tube local buckling. The occurrence of tube local buckling has an obvious detrimental effect on the fire resistance of CFST columns. In contrast, the steel tube in a TRC column is mainly subject to tension in the transverse direction and so tube local buckling could generally be minimised or significantly delayed.

Compared to RC columns, the steel tube of TRC columns can effectively prevent the concrete cover from peeling off due to fire spalling and so help maintain the integrity of the concrete section and protect the re-bars against heating.

To the authors' knowledge, no study has been reported on the fire behaviour of square TRC columns so far. Motivated by the increasing applications of TRC columns in engineering practices, the authors conducted a series of studies on the fire performance and post-fire behaviour of TRC columns. Experimental and numerical studies on the fire performance of circular TRC columns were conducted and reported by Liu et al. [42]. It was found that the load ratio, cross-sectional dimension and slenderness ratio are the most important factors affecting the fire resistance of circular TRC columns. A simplified design method was also proposed for the prediction of the fire resistance of circular TRC columns [42]. The aim of this research is to study and reveal the fire behaviour of square TRC columns. Fire tests were conducted on five square TRC slender columns subjected to various load ratios and load eccentricities. The temperature distribution and high-temperature deformation, failure mode and fire resistance of these square TRC columns were obtained from the tests. The influences of load ratio and load eccentricity ratio were evaluated. A sequentially-coupled thermo-mechanical FEA model was then developed and validated against the experiments. The load redistributions within the composite section during heating and loading were analysed in order to reveal the working mechanism of square TRC columns exposed to fire.

2. Experimental investigation

2.1 Details of the specimens

Five slender square TRC columns were tested. Three specimens were subjected to concentric load; and the other two were eccentrically-loaded. The details of these specimens are reported in Table 2, including the sectional depth D, width B, tube thickness t_s and column length L. The symbols α and ρ in Table 2 represented the cross-section steel ratio (the area of steel tube over that of concrete) and reinforcement ratio (the area of steel reinforcement over that of concrete) of the column, respectively. Load ratio was found to be one of the most critical parameters that affect the fire performance of circular TRC columns [42]. Most composite columns in real engineering are under the combined effects of compression and bending, and so load eccentricity is also an important parameter. Thus, load ratio n and load eccentricity e were chosen as the key testing parameters in this paper, the values of which were used to name the specimens. For example, TRC-0.5-25 was corresponding to a specimen with a load ratio

= 0.5 and a load eccentricity = 25 mm. Axial load was applied onto the top of the column and maintained constant during the test. The value of the axial load N_f was obtained by the load ratio multiplying the ambient-temperature bearing capacity of the column that determined according to the Chinese design code JGJ/T471 [43]. Load ratios were 0.4, 0.5 and 0.6 considering the typical load levels of steel-concrete composite columns in the fire limit state [44]. Load eccentricity ratios (defined as $2e/D$) were taken as 0.2 and 0.4. As shown in Fig. 2(b), each column contained eight longitudinal reinforcements with a diameter ϕ of 16 mm, as well as 8 mm diameter stirrups at 200 mm spacing. Stirrups with a diameter of 10 mm were placed at 50 mm intervals near column ends. Concrete cover, i.e. the distance from the concrete surface to the outer edge of the stirrup, was 25 mm.

Each square steel tube was fabricated by welding two channel sections together. After placing the reinforcing cage into the steel tube centrally at the proper position, two end plates were welded to the bottom and top of the steel tube. A square hole was cut on the top end plate for concrete casting and then it was sealed. For eccentrically-loaded columns, the offset distance between the central lines of the end plates and steel tube section equalled to the load eccentricity.

In each fire test, an unloaded stub column of 400 mm height was placed next to the slender specimen to measure the temperature distribution across the cross-section. This measurement was believed to represent the temperature distribution within the loaded column, given that previous research conducted by Romero et al. [22] indicated that the applied load and the second-order effect barely affected the temperature distribution within a column. The uniformity of temperature distribution along the height of the furnace had already been verified in our previous testes [42]. All the cross-sectional details of these stub columns are the same as those of the slender columns. Type K (nickel-chrome) thermocouples were adopted for temperature measurements; their locations are illustrated in Fig. 2(c). The measuring points 1 and 6 were at the outer surface of the steel tube, points 2-5 were embedded in the concrete core and points 7-10 were at the re-bars.

2.2 Material properties

The steel tubes and reinforcing bars were made of mild steel. The ambient-temperature mechanical properties of the steel tube and re-bars were determined by tensile coupon tests according to ISO 6892-1 [45]. The test results are summarized in Table 3, including the steel tube yield strength f_y, re-bar yield strength f_b, ultimate strength f_u, elastic modulus E_s, Poisson's ratio v and elongation ratio ε_f.

Ready-mixed self-compacting concrete (SCC) was employed in the tests and the mix design is listed in Table 4. Grade 42.5 ordinary Portland cement and medium river sand with a fineness modulus of 2.5 were used and the coarse aggregate was calcareous bluestone with the grading of 5-20 mm. Mineral powder and fly ash were added as filler to improve the workability of the concrete. The measured slump flow was 700 mm. Concrete cubes of 100 mm width and 150 mm width and 150×150×300 mm prisms were cast and wrapped with tinfoil and then cured under the same condition as for the columns. The results of concrete cube compressive strength f_{cu} and elastic modulus E_c on 28 days and on the day of fire testing (190 days) are listed in Table 4. The moisture content of concrete was measured using three 100 mm cubes on the day of fire testing according to ISO 12570 [46] and the mean value was 5.4%.

2.3 Test setup and procedure

A furnace, with inner dimensions of 4200×1900×4050 mm, was used to heat the specimens. The furnace temperature-time relationship followed the ISO 834 standard fire curve. Ten gas burners were embedded at different locations of the chamber. Eight type S (platinum-rhodium) thermocouples were employed to measure the furnace air temperatures.

Each slender column was nominally pinned about the y-axis (shown in Fig. 2(b)) at both ends with a slenderness ratio λ ($\lambda=2\sqrt{3}L/D$) of 52.8. This one-direction pinned boundary condition was also used in the fire tests reported in [42,47-52]. The column ends about the x-axis were fixed. The heated length of a column was 3000 mm. Right above and below the heated zone, two gaps of 30 mm width were cut as shown in Fig. 2(a). These gaps were also used to release steams due to moisture vaporization in concrete.

A hydraulic jack with a maximum loading capacity of 3000 kN was used to load the specimens. The slender column was erected in the test rig and then preloaded to 100 kN until all the bolts were fastened. The unloaded stub column was located next to the slender column. The slender column was loaded to the designated load N_f with an interval of 20%N_f and then the axial load was kept constant by the automatic control system. Then gas burners were ignited and the column was heated under constant load until the axial deformation or axial deformation rate reached the criteria described in ISO 834-1 [53]. The corresponding failure time was defined as fire resistance. The test procedure of column TRC-0.4-0 is displayed in Fig. 3(a) as an example. The measured axial load-time curve of this specimen is illustrated in Fig. 3(b) and a good precision of the automatic control system was achieved.

To measure the lateral deformation at the mid-height of the heated part of a specimen, two wires were first fixed to the column surfaces and then connected to two vertical LVDTs out of the furnace through fixed pulleys. More details of this measurement method can be found in reference [52]. The displacement of a column during the fire test was the total displacement subtracting the displacement due to ambient-temperature loading, in order to exclude the influence of test rig deformations. Fig. 4 shows the test setup, including (1) the gas furnace, (2) the steel reaction frame, (3) the location of tested slender column, (4) the locations of furnace thermocouples, (5) the hydraulic jack, (6) the layout of axial LVDTs, (7) top boundary condition and (8) bottom boundary condition. As shown in Fig. 4(c), there were a total of eight vertical LVDTs (named by u_1-u_8) to check the deformation uniformity of the top loading device, four of which were located at the upper steel plate connected to the hydraulic jack and the other four were located at the lower steel plate with bolt holes. Two of the LVDTs u_4 and u_7 are not visible in Fig. 4(c); they are in the symmetrical locations to u_3 and u_8. It should be noted that although the loading bearing was lubricated before each test, it was still impossible to generate an ideal pinned boundary due to the inevitable friction. The measured rotation-time relationships of the top end plate could be used to reflect the real boundary condition and this will be discussed hereinafter.

3 Test results and discussions

3.1 Failure modes

The failure criterion of axial displacement rate in ISO 834-1 [53] was reached with a value of 0.003L mm/min (11.43 mm/min in this paper). Then the columns were unloaded and all the burners were turned off. Most of the columns experienced global buckling failure except the column TRC-0.6-0 that failed by concrete crushing and buckling of re-bars in compression. This compression failure was also observed in previous research on CFST columns conducted by Lie and Chabot [54-55], Kodur and Latour [56], Wang and Young [57] and Xiong and Liew [58]. The typical failure modes of the columns after unloading are presented in Fig. 5. The midspans of the columns exhibited obvious lateral deformations and the column-end rotations were considerable. Though designed not to carry any axial loads directly, the steel tube of the square TRC column experienced local buckling especially in the column mid-height, which is in accordance with the findings in the fire tests of circular TRC columns [42] and the post-fire tests of circular and square TRC columns [59-62]. The occurrence of tube local buckling may be due to the axial stress in the steel tube caused by the inevitable bond and friction at the steel-concrete interface. Generally, this axial stress accumulates from the column end to the mid-height [63].

Post-fire deformations of the specimens including the residual column lengths L_{res}, residual end plate rotations $\varphi_{\mathrm{res,top}}$ and $\varphi_{\mathrm{res,bot}}$, maximum residual lateral deformations w_{max} and the corresponding location heights x_{max} are displayed in Fig. 5 except for TRC-0.6-0. These residual deformations were smaller than the real deformations of the columns at the end of the fire tests due to the deformation-recovery caused by cooling and unloading. Fig. 5(f) shows the two cutting gaps of specimen TRC-0.4-0 after fire test. The concrete cover within these gaps was crushed due to the lack of steel tube confinement. Although these gaps narrowed due to the compression deformation of the confined RC section and the thermal expansion of the steel tube, the gaps were not eliminated.

After the fire tests, the outer steel tubes were removed to examine the inner concrete cores and re-bars. For the specimen TRC-0.5-25, the concrete in the compression zone at mid-height was crushed together with the buckling of the reinforcements at the same location and apparent transverse cracking was observed in the corresponding tension zone, as shown in Figs. 6(a)-6(c). It can be seen from Figs. 6(d)-6(f) that the column TRC-0.6-0 failed by local concrete crushing and all the longitudinal reinforcements buckled by compression at the same location.

3.2 Temperature histories

The measured temperature curves of the furnace thermocouples (T1-T8) during the fire test of TRC-0.4-0 was compared with the standard ISO 834 curve in Fig. 3(c). The spatial distribution of the furnace temperature was uniform and the use of unloaded stub columns to measure the temperature distribution within the slender columns was feasible. The average furnace air temperature-time curves of all the tests are summarized in Fig.

7(a), which shows a good precision of furnace air temperature control.

As shown in Figs. 7(b)-7(h), a good uniformity of the temperature fields within these specimens was substantiated. The differences between these curves in Fig. 7(b) may be attributed to that the fire insulation measures to some of the steel tube thermocouples were not tight enough and these thermocouple results were affected by the flames. Though tips of thermocouples 1 and 6 had been wrapped locally with insulation material. Symmetric measuring points of re-bars generally presented close temperature measurements, which revealed the uniformity of heating between different faces of a column. Re-bars at the cross-section corners (Points 8 and 9 in Fig. 2(c)) were hotter than those at the edge midpoints (Points 7 and 10 in Fig. 2(c)), which was caused by different dimensionalities of heat transfer. Visible temperature plateau in concrete occurred at around 100-150 ^{o}C due to the water evaporation and migration.

3.3 Deformation behaviour

The mean axial displacement of specimen TRC-0.4-0, measured from eight vertical LVDTs u_1-u_8 in Fig. 4(c), is shown in Fig. 3(d). The graph legends of Fig. 3(d) indicate which LVDTs are considered to obtain the mean displacement values; for example, Ave(u_1,u_2) is the average of the LVDTs u_1 and u_2. The overlapping of curves Ave(u_1,u_2) and Ave(u_3,u_4) indicates the upper loading plate moved vertically and maintained horizontal without rotation. There were obvious differential displacements between Ave(u_5,u_6) and Ave(u_7,u_8), due to the lower steel plate rotation $\varphi(t)$, which was taken as the difference between Ave(u_5,u_6) and Ave(u_7,u_8), divided by the distance between LVDTs u_5 and u_7. Ave(u_1,u_2,u_3,u_4) and Ave(u_5,u_6,u_7,u_8) were similar, indicating that the deformation of the test rig between the lower and upper steel plates had little influence on the measured specimen axial displacement. The axial displacement of each column was finally taken as Ave(u_5,u_6,u_7,u_8).

The deformation-time relationships of the specimens are summarized in Fig. 8, including the axial deformation $u(t)$ and lateral deformation $w(t)$. Positive vertical deformations correspond to axial elongation and negative ones were for the column shortening. The influence of the thermal expansions of the two wires used to measure the specimen lateral deformation was removed by averaging the measured deformation of these two wires, as described in reference [52]. The lateral deformation of TRC-0.4-0 was not recorded to failure because the wires broke prematurely. All columns failed by exceeding the limit of the axial deformation rate. The fire resistance t_{FR} of the specimens were marked using red dots in Fig. 8 and the results of t_{FR} for these five specimens are included in Table 2. The temperature reached by the steel tube at failure time was defined as limiting temperature. Although the limiting temperature of steel tube alone should not be able to define the fire resistance of TRC columns, it can reflect the influence of fire on the TRC columns to some extent.

3.4 Discussions of results

The fire behaviour of square TRC columns is the combined effects of two phenomena, (1) axial elongation due to thermal expansion and (2) axial shortening caused by temperature-induced material degradation under loading. Depending on which phenomenon dominates, the evolution of the column axial displacement with time can be divided into several phases. As shown in Fig. 8, the axial deformation of specimens TRC-0.4-0, TRC-0.5-0 and TRC-0.5-25 experienced three phases: Phase 1 - elongation, Phase 2 - shortening and Phase 3 - failure. During Phase 1, the heating rate was high and the effect of thermal expansion was dominant. The durations of axial elongation for these three columns were 50.5 min, 2.2 min and 40.7 min, respectively and the corresponding maximum expansion values were 0.47 mm, 0.09 mm and 0.39 mm. With further heating, the material properties degraded notably as the specimen temperature increased, causing axial contraction under loading which dominated over the thermal expansion. This phase is defined as Phase 2. In Phase 3, as the materials degraded further with the temperature rising, when the resistance of the column fell below the applied load, failure occurred and an abrupt increase of the axial deformation was recorded. Due to the large load ratio, specimen TRC-0.6-0 only underwent crushing failure in compression. For column TRC-0.5-50, the axial deformation experienced four phases, which started from shortening, switched to elongation and then returned to shortening before failure. The first contraction phase last about 9 min and the maximum compressive deformation was only 0.2 mm. Apart from the possible influence of measurement errors, the occurrence of this phase may be attributed to the second-order effect caused by large eccentricity.

3.4.1 Effect of load ratio

The influence of load ratio on the axial deformation, lateral deformation, endplate rotation, steel tube limiting temperature and fire resistance of the tested square TRC columns are plotted in Figs. 9(a)-9(d). The column with larger load ratio experienced larger axial compression deformation, mid-span lateral deformation and endplate rotation at the same fire exposure time. Fig. 9(b) shows that the lateral displacement of specimen TRC-0.6-0 is considerate and of the same order as for the other specimens, whereas Fig. 5(c) shows that this specimen being quite straight after testing. The reason might be that most of the global lateral deformation of this column recovered after cooling and unloading.

The fire resistance of concentrically-loaded columns decreases from 86.7 min to 38.1 min, as load ratio increases from 0.4 to 0.5. The fire resistance of the specimen TRC-0.6-0 is only 13.5 min. The obtained steel tube limiting temperatures of these three TRC columns subject to load ratios 0.4, 0.5 and 0.6 are 917.6 ^{o}C, 760.5 ^{o}C and 454.9 ^{o}C, respectively. It is interesting to find in Fig. 9(d) that the increase of fire resistance is not proportional to the load ratio decrease. For instance, comparing specimens TRC-0.6-0 and TRC-0.5-0, the fire resistance increases by 181.7% when the load ratio decreases by 16.7%. When the load ratio decreases from 0.5 to 0.4 (20%), the improved level of fire resistance is 127.5%. Compared to the apparent increasing levels of fire resistance (181.7% and 127.5%), the corresponding increase levels in the limiting temperatures of steel tube are only 67.2% and 20.7%. This is due to the continuously decreasing heating rate of the ISO 834 standard fire, i.e. the rate at 13.5 min is 11 ^{o}C/min and decreases to only 1.7 ^{o}C/min at 86.7 min.

3.4.2 Effect of load eccentricity

As presented in Figs. 9(e)-9(h), the overall lateral deformation of the column and the endplate rotation generally increase with the increasing of load eccentricity. At the same heating time, the columns under eccentric load generally experienced smaller axial compressive deformation than the concentrically-loaded specimen. In terms of fire resistance, TRC-0.5-25 with a medium eccentricity of 25 mm obtained the longest fire resistance 45.5 min compared to specimens TRC-0.5-0 (38.1 min) and TRC-0.5-50 (35.6 min). The corresponding limiting temperatures of steel tube are 760.5 ^{o}C, 772.5 ^{o}C and 694.3 ^{o}C, respectively.

Within the research scope of this paper, the influence of load eccentricity on the fire resistance of the specimens subject to the same load ratio 0.5 is found to be modest. On one hand, the existence of load eccentricity increases the second-order effect and decreases the high-temperature load-bearing capacity of the column, which might lead to the decrease of fire resistance. On the other hand, under the same load ratio, the applied load on an eccentrically-loaded column is lower than that on a concentrically-loaded column, which would be beneficial for the fire resistance of the former. Compared with the concentrically-loaded specimen TRC-0.5-0, the fire resistance increases by 19.2% and -6.9% respectively for columns with load eccentricity ratios of 0.2 and 0.4, as the applied loads decrease by 31.4% and 47.5%. This indicates that the load eccentricity ratio of 0.2 has a positive effect on fire resistance whereas a larger load eccentricity ratio 0.4 results in a lower fire resistance.

4. Numerical simulations

A sequentially-coupled thermal-stress analysis model was built using the program ABAQUS [64]. The mesh sizes adopted for the heat transfer and stress analyses were the same. The measured specimen dimensions, material properties, applied loads and furnace temperature-time relationships were adopted in the FEA modelling. Considering the symmetries in the experiments, only half of the composite cross-section was built.

4.1 Thermal analysis

For the heated faces of the column, a convective coefficient of 25 W/(m^2·K) was adopted and a comprehensive emissivity coefficient of 0.5 that recommended by ECCS 1988 [65] was used. This emissivity value was found to give accurate predictions for fire experiments of composite columns [42,52,59-62,66-71]. For the part of the specimen which was out of the furnace, there was conduction from the heated part of the specimen, followed by radiation and convection to the environment. This was considered by adopting a convective coefficient of 9 W/(m^2·K), which also included the effects of radiation, as given in EC1 [72]. For the parts of the specimen that were in the furnace but thermally insulated, it was assumed that there was only conduction from the heated part. The thermal models of concrete and steel that recommended by ASCE [73] and EC2 [74] have been successfully used for simulations of CFST columns by many researchers and these two models are expected to yield good predictions in the thermal simulation of TRC columns. The ASCE model is the same as that proposed by Lie [75] and it has been used to predict the thermal response of circular TRC columns [42]. Therefore, the ASCE model was still used in the paper. The measured moisture content was considered in the calculation of the specific heat of concrete to reflect the influence of water evaporation. A thermal resistance of 0.01($m^2 \cdot K$)/W was considered at the steel-concrete interface, as recommended by Ding and Wang [66] and Lv et al. [76]. The nodes of the re-bars were tied to those of concrete at the same locations. The element types were DC3D8, DS4 and DC1D2 for concrete, steel and reinforcements, respectively.

As shown in Fig. 10, the thermal analysis model was validated against the measured temperatures of the tested specimens. The FEA results matched very well with the experimental data, especially for the temperatures of the steel tube and re-bars. The discrepancy between the predicted and measured concrete temperatures may be caused by: 1) the thermocouples may be slightly misplaced; 2) the ASCE thermal models of concrete may be different from those of the SCC used in the test; and 3) the moisture movement inside concrete was not considered in the model.

The heat transfer analysis was further validated against experiments of circular TRC columns conducted by Liu et al. [42]. These experiments are the most relevant to this study. The modelling and test results agreed well with each other, as shown in Figs. 11(a)-11(b).

4.2 Mechanical analysis

In the mechanical analysis, the concrete damage plasticity (CDP) model was employed for concrete. In the CDP model, the dilation angle is 36 $^{\circ}$ and the default values for the flow potential eccentricity, the ratio of the second stress invariant on the tensile meridian and the viscosity parameter, given in the ABAQUS manual, were adopted. As for the ratio of initial equibiaxial compressive yield stress to initial uniaxial compressive yield stress, the temperature-dependent formula proposed by Gernay et al. [77] was used. The temperature-dependent constitutive model for concrete in compression given by Lie [72], which is the basis of the ASCE [73] model, was used in this paper. This model is presented as the $\sigma_{cc,T}$-$\varepsilon_{cc,T}$ relationship in Eq. (1). As for the high-temperature tensile constitutive model of concrete, the stress-strain relationship $\sigma_{ct,T}$-$\varepsilon_{ct,T}$ recommend by Hong and Varma [21] was adopted, which is shown in Eq. (2). The high-temperature stress-strain relationship for hot rolled reinforcing steel given in EC2 [74] and that for carbon steel given in EC3 [78] were employed in this study. The EC2 and EC3 equations (Eq. (3)) are identical. The only difference between the two is in the values of the high-temperature reduction factors, i.e. the slope of the linear elastic range E_{sT}, the proportional limit f_{pT} and the effective yield strength f_{yT}. It should be noted that the transient strain and creep of concrete and the creep of steel were implicitly included in these material models.

$$\sigma_{\mathrm{cc,T}}=\begin{cases} f_{\mathrm{cT}}^{'}\left[1-\left(\dfrac{\varepsilon_{\max}-\varepsilon_{\mathrm{cc,T}}}{\varepsilon_{\max}}\right)^2\right] & \varepsilon_{\mathrm{cc,T}}\le\varepsilon_{\max} \\ f_{\mathrm{cT}}^{'}\left[1-\left(\dfrac{\varepsilon_{\mathrm{cc,T}}-\varepsilon_{\max}}{3\varepsilon_{\max}}\right)^2\right] & \varepsilon_{\mathrm{cc,T}}>\varepsilon_{\max} \end{cases} \tag{1}$$

where $f_{\mathrm{cT}}^{'}=\begin{cases} f_{\mathrm{c}}^{'} & 0°\mathrm{C}<T<450°\mathrm{C} \\ f_{\mathrm{c}}^{'}\left[2.011-2.353\left(\dfrac{T-20}{1000}\right)\right] & 450°\mathrm{C}\le T\le 874°\mathrm{C} \\ 0 & T>874°\mathrm{C} \end{cases}$, $f_{\mathrm{c}}^{'}$ is the cylinder compressive strength of concrete at room temperature, $\varepsilon_{\max}=0.0025+(6T+0.04T^2)\times10^{-6}$.

$$\sigma_{\mathrm{ct,T}}=\begin{cases} E_{\mathrm{cT}}\varepsilon_{\mathrm{ct,T}} & \varepsilon_{\mathrm{ct,T}}\le\varepsilon_{\mathrm{cr}} \\ f_{\mathrm{tT}}^{'}-0.1f_{\mathrm{tT}}^{'}\dfrac{\varepsilon_{\mathrm{ct,T}}-\varepsilon_{\mathrm{cr}}}{\varepsilon_{\mathrm{cr}}} & \varepsilon_{\mathrm{cr}}<\varepsilon_{\mathrm{ct,T}}\le 2\varepsilon_{\mathrm{cr}} \\ 0.9f_{\mathrm{tT}}^{'} & \varepsilon_{\mathrm{ct,T}}>2\varepsilon_{\mathrm{cr}} \end{cases} \tag{2}$$

where $f_{\mathrm{tT}}^{'}=0.09f_{\mathrm{cT}}^{'}$, $\varepsilon_{\mathrm{cr}}=f_{\mathrm{tT}}^{'}/E_{\mathrm{cT}}$.

$$\sigma_{\mathrm{sT}}=\begin{cases} E_{\mathrm{sT}}\varepsilon_{\mathrm{sT}} & \varepsilon_{\mathrm{sT}}\le\varepsilon_{\mathrm{pT}} \\ f_{\mathrm{pT}}-c+\dfrac{b}{a}\sqrt{a^2-(\varepsilon_{\mathrm{yT}}-\varepsilon_{\mathrm{sT}})^2} & \varepsilon_{\mathrm{pT}}<\varepsilon_{\mathrm{sT}}\le\varepsilon_{\mathrm{yT}} \\ f_{\mathrm{yT}} & \varepsilon_{\mathrm{yT}}<\varepsilon_{\mathrm{sT}}\le\varepsilon_{\mathrm{tT}} \\ f_{\mathrm{yT}}\dfrac{1-(\varepsilon_{\mathrm{sT}}-\varepsilon_{\mathrm{tT}})}{\varepsilon_{\mathrm{uT}}-\varepsilon_{\mathrm{tT}}} & \varepsilon_{\mathrm{tT}}<\varepsilon_{\mathrm{sT}}<\varepsilon_{\mathrm{uT}} \\ 0 & \varepsilon_{\mathrm{sT}}=\varepsilon_{\mathrm{uT}} \end{cases} \tag{3}$$

where $\varepsilon_{\mathrm{pT}}=f_{\mathrm{pT}}/E_{\mathrm{sT}}$, $\varepsilon_{\mathrm{yT}}=0.02$, $\varepsilon_{\mathrm{tT}}=0.15$, $\varepsilon_{\mathrm{tT}}=0.2$, $a^2=(\varepsilon_{\mathrm{yT}}-\varepsilon_{\mathrm{pT}})(\varepsilon_{\mathrm{yT}}-\varepsilon_{\mathrm{pT}}+c/E_{\mathrm{sT}})$,

$b^2=c(\varepsilon_{\mathrm{yT}}-\varepsilon_{\mathrm{pT}})E_{\mathrm{sT}}+c^2$, $c=\dfrac{(f_{\mathrm{yT}}-f_{\mathrm{pT}})^2}{(\varepsilon_{\mathrm{yT}}-\varepsilon_{\mathrm{pT}})E_{\mathrm{sT}}-2(f_{\mathrm{yT}}-f_{\mathrm{pT}})}$.

The temperature-dependent equation for the concrete Poisson's ratio proposed by Gernay et al. [77] was adopted in the analysis. The thermal expansion coefficient of concrete was assumed to be constant, which is $6\times10^{-6}/^{\circ}\mathrm{C}$, as adopted by Hong and Varma [21], Liu et al. [42] and Espinos et al. [79]. The temperature-dependent thermal expansion coefficients recommended in EC3 [78] were used for the steel tube and reinforcement bar. General surface-to-surface contact, with a friction coefficient of 0.3, was used for the steel-concrete interface. The re-bars were embedded into the concrete to achieve the deformation compatibility. An initial imperfection with the value of 1/1000 of the column length was included and the corresponding shape was the first buckling mode. Element types C3D8R, S4R and T3D2 were used to model concrete, steel tube and re-bar, respectively. In the FEA, the failure of the column was defined based on the same failure criteria as for the testing.

As discussed in Section 2.3, an ideal pinned boundary condition is difficult to realize and the actual boundary condition of the testing should involve a certain degree of rotational restraint. To evaluate the impact of the column-end rotational restraint, three different boundary conditions, i.e. pinned, fixed and the measured experimental rotation-time relationship $\varphi(t)$ were adopted in the FEA. The modelling results are shown in Figs. 12(a)-12(e). In the pinned boundary condition, the column top is only free to rotate in one direction (i.e. rotate about the y-axis in Fig. 2(b)) and move along the axial direction; the column bottom is assumed to rotate only about the y-axis of the column cross-section. As for the fixed boundary condition, the column top is only free to move along the longitudinal axis; all the other degrees of freedom of the column bottom end are restricted. When the measured column end rotation-time relationship is adopted as the boundary condition, the column top could only move along the axial direction and rotate about the cross-section's y-axis; the column bottom is only able to rotate about the y-axis. The measured $\varphi(t)$ curve in Fig. 9(c) or Fig. 9(g) is set as the amplitude of the column rotation in ABAQUS. The rotation of the column bottom end was not measured during the fire test and it was assumed to be the same as the measured rotation of the column top end, since the measured post-fire column-end rotations at the top and bottom were almost identical, as shown in Fig. 5. It can be found from Fig. 12 that the test fire resistance lies between the FEA results of pinned and fixed boundary conditions. The actual $\varphi(t)$ relationship can be used as the real boundary condition and a similar simulation approach was also employed by Neuenschwander et al. [80]. The lateral-displacement-time relationships given by FEA were also compared with the test results in Figs. 12(f)-12(j) and a pretty good agreement was achieved. As a typical example, the failure mode of specimen TRC-0.5-50 given by the FEA modelling is illustrated in Fig. 5(e), together with the test pictures. The nonlinear FEA model can capture both the global buckling of the whole specimen and the local buckling of the steel tube.

The mechanical FEA model was further validated against the measured axial displacement-time curves of circular TRC columns [42], as illustrated in Figs.

11(c)-11(d). Moreover, the fire resistance of a total of 84 composite columns, including five square TRC columns tested in this research, four circular TRC columns in [42], 21 square CFST columns from the experiments conducted by Han et al. [47], Espinos et al. [48] and Lie and Chabot [54-55] and 54 circular CFST columns reported by Espinos et al. [48], Moliner et al. [50], Lie and Chabot [54-55] and Han et al. [81] were modelled and the results are in Fig. 11(e). The details of these fire tests on TRC and CFST columns and the comparison of the fire resistance between the FEA predictions and the test results are summarized in Table 5. The mean value of the ratio between the modelled fire resistance $t_{\mathrm{FR,FE}}$ and measured one $t_{\mathrm{FR,test}}$ is 1.05 and the standard deviation is 0.18, indicating a good agreement considering the complexity and results variability of fire tests.

4.3 Load redistribution analysis

During the fire exposure, the non-uniform temperature distribution within the column cross-section causes different thermal expansions and material degradations. As a result, the axial load resisted by the column will be redistributed within the composite section. The load redistribution within the mid-span cross-section of square TRC columns in fire is analysed using the FEA model in Section 4.2. Axial force ratio is defined as the axial force of concrete, steel tube or re-bars over that of the whole cross-section. Fig. 13(a) shows the axial force ratio-time curves for concrete core, reinforcement and steel tube of specimen TRC-0.5-0. The axial force in the steel tube is small though there are bond stress and friction between the steel tube and concrete core. The axial force ratio of the concrete core decreases from 82.3% to 64.5% and then keeps almost constant. Simultaneously, the axial force born by the reinforcements firstly increases and then remains almost unchanged. This load redistribution may be caused by the fact that heating causes the decrease of the stiffness of the outer concrete layers and thus increases the strain of concrete, resulting in the increase of the longitudinal strains of the re-bars as plane cross-sections remain plane. Fig. 13(b) shows the development of normalized stress over time during heating for reinforcement bars at different locations. S_{b} is the longitudinal stress of re-bar (the positive value of S_{b} corresponds to tensile stress). f_{bT} is the high-temperature yield strength of the reinforcement and it is equal to the ambient-temperature strength, since all the reinforcement temperatures do not exceed 300 $^{\mathrm{o}}$C throughout this test. All the longitudinal stresses in the re-bars increase almost linearly in the first 20 min of heating until yielding occurs. After that, the stresses of the re-bars in the tension zone of the cross-section decrease slightly, which is caused by the increasing second-order effect.

The axial stresses of six concrete nodes at different fire exposure moments are plotted in Fig. 13(c), in which positive value represents tensile stress. The whole concrete section is under compression after the ambient-temperature loading and the axial stress along the x-axis distributes linearly since the section remains plane. During the heating process, the stress evolution of a certain node is affected by the high-temperature material degradation as well as the differential thermal stresses that caused by the non-uniform temperature distribution of the concrete section. The outer concrete layers near the steel surface are under thermal compressive stresses while the inner layers are under tension. The stress of node 1 is always the highest during the heating followed by that of node 6. The increase of the compressive stress of node 6 until 10 min heating is mainly caused by the increase of thermal compressive stress and the continual stress decrease in the later stage of exposure is due to the increasing second-order effect and the material degradation. The compressive stresses of inner nodes 3 and 4 keep decreasing until 30 min exposure, which is a result of the increasing thermal tensile stress. After that, here occur compressive stress increases in these two nodes since the elastic modulus of the outer concrete layers decrease significantly and the axial load is gradually transformed to the inner layers.

As presented in Fig. 14(a), the evolutions of the load redistributions of specimens TRC-0.4-0, TRC-0.5-0 and TRC-0.6-0 follow similar patterns. The axial load is continuously redistributed from concrete to re-bars until the reinforcements yield. Before reinforcement yielding, a higher load ratio leads to a higher percentage of axial force in the re-bars, indicating a higher contribution of re-bars to the total load-bearing capacity. However, the reinforcements also yield earlier in columns subject to higher load ratio and the load redistribution stops when yielding occurs. The load redistribution in specimen TRC-0.4-0 lasts for the longest time, and so the final axial force ratio of re-bars is also the highest. For specimen TRC-0.4-0, the force in concrete recovers slightly towards the end of heating. This may be due to the strength loss of the re-bars after long heating and so part of the load is transferred back to the concrete core. For the columns TRC-0.5-0, TRC-0.5-25 and TRC-0.5-50, the axial force ratio-time curves are almost the same in the early stage of fire exposure, as shown in Fig. 14(b). It is obvious that and the axial load in the eccentrically-loaded columns is transferred back to concrete in the latter stage of heating. This phenomenon is attributed to the influence of the bending moment caused by load eccentricity and increasing second-order effect. The re-bars in the compression zone yield while the ones in the tension zone undergo obvious stress drops.

The fire behaviour of a CFST column was compared with that of a TRC column to illustrate the difference of fire performance between these two composite members. The infill of the CFST column was bar-reinforced concrete since the load distribution within this kind of CFST column could also occur among the steel tube, concrete core and re-bars, which is comparable with the case of the TRC column. The load ratio of the TRC column was 0.5 and the CFST column had the same applied load as the TRC column. Compared to the TRC column, the steel ratio of the CFST column was increased from 3.62% to 8.0%, a value within the common range 4%-20% for CFST columns. Other details of these two columns were all the same as those of the test TRC specimens in Section 2. Simply-pinned boundary conditions were employed in the simulation. The results of the axial deformation-time curves and the sectional load redistributions in the heating procedure are displayed in Figs. 15(a)-15(b). The CFST column had a higher fire resistance than the TRC column, which may be explained by the lower load ratio for the CFST column. Different from the axial deformation behaviour of the square TRC columns that discussed in Section 3.4, the axial deformation curve of the CFST column generally consists of four stages and there was a separation in the axial direction between the steel tube and the RC section in the first 3 min of the heating. This was consistent with the findings reported by Espinos et al. [79]. The axial load redistribution in a TRC column generally occurred only within the concrete and the re-bars. However, the axial load applied to a CFST column was first transferred to the steel tube and then gradually transferred back to the inside RC section, as shown in Fig. 15(b). For both of these two columns, the axial load was mainly sustained by the RC section at the failure stage.

To clarify the fire performance difference between TRC columns and CFST columns further, two columns of 400 mm width were analysed and the results are shown in Figs. 15(c)-15(f). These two columns were subject to the same axial load, 0.5 times of the ambient-temperature bearing capacity of the TRC column. The steel ratios of the TRC column and CFST column were 3% and 8%, respectively. As shown in Figs. 15(e)-15(f), both the TRC column and CFST column failed mainly by global buckling. The steel tube local buckling of the TRC column was slight and mainly occurred at the concave side of the column mid-height. For the CFST column, considerable tube local buckling occurred at the mid-height and two ends of the column on all four sides. This may be because that the steel tube in this CFST column sustained up to 86% of the axial load in its expanding stage. Contrary to the comparison result in Fig. 15(a), fire resistance of the CFST column was shorter than that of the TRC column, which may be caused by the negative influence of severe tube local buckling.

5. Conclusions

Five slender square tubed-reinforced-concrete columns were tested under combined thermal and mechanical actions. A FEA model was developed and validated against experimental results. Based on the experimental and numerical work conducted, the following conclusions can be drawn.

1) The main failure mode of the tested square TRC columns in fire is global buckling, together with slight local buckling of the steel tube. At the mid-height of the columns, concrete is crushed and steel reinforcements buckle in the compression zone; and transverse cracks of concrete are observed in the corresponding tension zone.

2) The development of the axial deformation of the tested square TRC columns generally consists of three phases, elongation, shortening and failure. Runaway failure is observed in most specimens. Fire resistance of the tested square TRC columns decreases significantly with the increase of load ratio from 0.4 to 0.6 and the effect of load eccentricity on fire resistance is unobvious.

3) The column end rotations measured during the experiments can be used to represent the realistic boundary conditions of the test specimens. The use of the measured column end rotations, instead of ideal pinned or fixed condition, as the boundary conditions of the numerical model considerably improves the agreement between the modelling and test results.

4) Through the load redistribution analysis on the FEA model, it is found that the axial load is gradually transferred from the concrete core to the steel reinforcements during heating. Before the steel reinforcements yield, a higher percentage of load is redistributed to the reinforcements as load ratio increases, whereas the case is opposite after reinforcements yielding. Load eccentricity does not affect the load redistribution in the early stage of heating, but the load will be transferred back to concrete in the later stage of heating for specimens under eccentric load.

Acknowledgements

The research work in this paper is financially supported by the National Natural Science Foundation of China (51978209) and the Foundation of Key Lab of Structures Dynamic Behaviour and Control of the Ministry of Education, Harbin Institute of Technology (HITCE201610), to which the authors are grateful.

Reference

[1] J.P. Liu, X.D. Wang, S.M. Zhang, Behavior of square tubed reinforced-concrete short columns subjected to eccentric compression, Thin-Walled Struct. 91 (2015) 108-115.

[2] X.H. Zhou, J.P. Liu, X.D. Wang, Y.F. Chen, Behavior and design of slender circular tubed-reinforced-concrete columns subjected to eccentric compression, Eng. Struct. 124 (2016) 17-28.

[3] EN 1994-1-1, Eurocode 4 - Design of Composite Steel and Concrete Structures - Part 1-1: General Rules and Rules for Buildings, CEN, Brussels, 2004.

[4] M. Tomii, K. Sakino, K. Watanabe, Y. Xiao, Lateral load capacity of reinforced concrete short columns confined by steel tube, Proceedings of the International Speciality Conference on Concrete Filled Steel Tubular Structures, Harbin, China (1985), 19-26

[5] M. Tomii, K. Sakino, Y. Xiao, K, Watanabe, Earthquake resisting hysteretic behavior of reinforced concrete short columns confined by steel tube, Proceedings of the International Speciality Conference on Concrete Filled Steel Tubular Structures, Harbin, China (1985), 119-125

[6] K. Sakino, M. Tomii, K. Watanabe, Sustaining load capacity of plain concrete stub columns confined by circular steel tube, Proceeding of the International Speciality Conference on Concrete Filled Steel Tubular Structures, Harbin, China (1985), 112-118.

[7] R.S. Aboutaha, R.I. Machado, Seismic resistance of steel-tubed high-strength reinforced-concrete columns, J. Struct. Eng. 125 (5) (1999) 485-494.

[8] L.H. Han, G.H. Yao, Z.B. Chen, Q. Yu, Experimental behaviours of steel tube confined concrete (STCC) columns, Steel Compos. Struct. 5 (6) (2005) 459-484.

[9] L.H. Han, H. Qu, Z. Tao, Z.F. Wang, Experimental behaviour of thin-walled steel

tube confined concrete column to RC beam joints under cyclic loading, Thin-Walled Struct. 47 (8-9) (2009) 847-857.
[10] S.M. Zhang, J.P. Liu, Seismic behavior and strength of square tube confined reinforced-concrete (STRC) columns, J. Constr. Steel Res. 63 (9) (2007) 1194-1207.
[11] J.P. Liu, S.M. Zhang, X.D. Zhang, L.H. Guo, Behavior and strength of circular tube confined reinforced-concrete (CTRC) columns, J. Constr. Steel Res. 65 (7) (2009) 1447-1458.
[12] Q. Yu, Z. Tao, W. Liu, Z.B. Chen, Analysis and calculations of steel tube confined concrete (STCC) stub columns, J. Constr. Steel Res. 66 (1) (2010) 53-64.
[13] J.A. Abdullah, S.M. Zhang, J.P. Liu, Shear strength and behavior of tubed reinforced and steel reinforced concrete (TRC and TSRC) short columns, Thin-Walled Struct. 48 (3) (2010) 191-199.
[14] X.H. Zhou, J.P. Liu, Seismic behavior and shear strength of tubed RC short columns, J. Constr. Steel Res. 66 (3) (2010) 385-397.
[15] X.D. Wang, J.P. Liu, S.M. Zhang, Behavior of short circular tubed-reinforced-concrete columns subjected to eccentric compression, Eng. Struct. 105 (2015) 77-86.
[16] Zhou XH, Liu JP. Performance and design of steel tube confined concrete members. Beijing China: Science Press Ltd.; 2010 [in Chinese].
[17] W. Ferdous, T.D. Ngo, K.T. Nguyen, A. Ghazlan, P. Mendis, A. Manalo, Effect of fire-retardant ceram powder on the properties of phenolic-based GFRP composites, Compos. Part B-Eng. 155 (2018) 414-424.
[18] L.H. Han. Theory and practice of concrete-filled steel tubular structure (third edition), Science Press, Beijing (China) (2016) [in Chinese]
[19] T.T. Lie, V.K.R. Kodur, Fire resistance of steel columns filled with bar-reinforced concrete, J. Struct. Eng. 122 (1) (1996) 30-36.
[20] Y.C. Wang, Steel and composite structures, behaviour and design for fire safety, Spon Press, London (2002)
[21] S. Hong, A.H. Varma, Analytical modeling of the standard fire behavior of loaded CFT columns, J. Constr. Steel Res. 65 (1) (2009) 54-69.
[22] M.L. Romero, V. Moliner, A. Espinos, C. Ibañez, A. Hospitaler, Fire behavior of axially loaded slender high strength concrete-filled tubular columns, J. Constr. Steel Res. 67 (12) (2011) 1953-1965.
[23] Z. Tao, M. Ghannam, T.Y. Song, L.H. Han, Experimental and numerical

investigation of concrete-filled stainless steel columns exposed to fire, J. Constr. Steel Res. 118 (2016) 120-134.

[24] H. Yang, L.H. Han, Y.C. Wang, Effects of heating and loading histories on post-fire cooling behaviour of concrete-filled steel tubular columns, J. Constr. Steel Res. 64 (5) (2008) 556-570.

[25] M. Pagoulatou, T. Sheehan, X.H. Dai, D. Lam, Finite element analysis on the capacity of circular concrete-filled double-skin steel tubular (CFDST) stub columns, Eng. Struct. 72 (2014) 102-112.

[26] F.Q. Meng, M.C Zhu, B. Mou, B.J He, Residual strength of steel-reinforced concrete-filled square steel tubular (SRCFST) stub columns after exposure to ISO-834 standard fire, Int. J. Steel Struct. 19 (2019) 850-866.

[27] F.Q. Meng, M.C Zhu, G.C. Clifton, K.U. Ukanwa, J.B.P Lim, Performance of square steel-reinforced concrete-filled steel tubular columns subject to non-uniform fire, J. Constr. Steel Res. 166 (2020) 105909.

[28] S. Huang, I.W. Burgess, Effect of transient strain on strength of concrete and CFT columns in fire - Part 2: Simplified and numerical modelling, Eng. Struct. 44 (2012) 389-399.

[29] M. Yu, H.M. Xu, J.Q. Ye, Y. Chi, A unified interaction equation for strength and global stability of solid and hollow concrete-filled steel tube columns under room and elevated temperatures, J. Constr. Steel Res. 148 (2018) 304-313.

[30] Y.F. Yang, L. Zhang, X.H. Dai, Performance of recycled aggregate concrete filled square steel tubular columns exposed to fire, Adv. Struct. Eng. 20 (9) (2017) 1340-1356.

[31] Klingsch W, Haksever A, Walter R. Brandversuche an stahlbetonstützen, versuchsergebnisse und numerische analyse. sonderforschungsbereich 148, Brandverhalten von Bauteilen, Arbeitsbericht, 1975_1977, teil I, T.U. Braunschweig, Juli 1977.

[32] Lie TT, Woollerton JL. Fire resistance of reinforced concrete columns: Test results. IRC Internal Report No. 569. Ottawa (Ontario): National Research Council of Canada, Institute for Research in Construction, 1988.

[33] P. Vandevelde, J.C. Dotreppe, R. Baus, H. Lambotte, A. Bruls, R. Minne, D. van Nieuwenburgt, H. Lambottet, Experimental research on the determination of the main parameters affecting the behaviour of reinforced concrete columns under fire condition, Mag. Concrete Res. 49 (179) (1996) 117-127.

[34] Kodur VKR, Cheng FP, Wang TC, Latour JC, Leroux P. Fire resistance of high-performance concrete columns. IRC Internal Report No. 834. Ottawa (Ontario): National Research Council of Canada, Institute for Research in Construction, 2001.

[35] K.H. Tan, Y. Yao, Fire resistance of four-face heated reinforced concrete columns, J. Constr. Steel Res. 129 (9) (2003) 1220-1229.

[36] S. Bratina, B. Cas, M. Saje, I. Planinc, Numerical modelling of behaviour of reinforced concrete columns in fire and comparison with Eurocode 2, Int. J. Solids Struct. 42 (21-22) (2005) 5715-5733.

[37] B. Wu, Z. Hong, G.H. Tang, C. Wang, Fire resistance of reinforced concrete columns with square cross section, Adv. Struct. Eng. 10 (4) (2007) 353-369.

[38] A. Sadaoui, A. Khennane, Effect of transient creep on the behaviour of reinforced concrete columns in fire, Eng. Struct. 31 (9) (2009) 2203-2208.

[39] A.M.B. Martins, J.P.C. Rodrigues, Fire resistance of reinforced concrete columns with elastically restrained thermal elongation, Eng. Struct. 32 (10) (2010) 3330-3337.

[40] P. Bamonte, F. Lo Monte, Reinforced concrete columns exposed to standard fire: Comparison among different constitutive models for concrete at high temperature, Fire Safety J. 71 (2015) 310-323.

[41] M. Achenbach, G. Morgenthal, Extension of the Zone Method of Eurocode 2 for reinforced concrete columns subjected to standard fire, J. Struct. Fire Eng. 7 (2) (2016) 82-96.

[42] F.Q. Liu, Y.Y. Wang, L. Gardner, A.H. Varma, Experimental and numerical studies of reinforced concrete columns confined by circular steel tubes exposed to fire, J. Struct. Eng. 145 (11) (2019) 04019130.

[43] JGJ/T471, Technical Standard for Steel Tube Confined Concrete Structures, MOHURD (Ministry of Housing and Urban-Rural Development of the People's Republic of China), Beijing, China, 2020 [In Chinese]

[44] A.H. Buchanan, A.K. Abu, Structural design for fire safety, John Wiley & Sons, New Zealand (2017) 124-126.

[45] ISO 6892-1, Metallic Materials-Tensile Testing, Part 1: Method of Test at Room Temperature, International Organization for Standardization ISO 6892, Geneva, Switzerland, 2016.

[46] ISO 12570, Hygrothermal Performance of Building Materials and Products-Determination of Moisture Content by Drying at Elevated Temperature,

International Organization for Standardization ISO 12570, Geneva, Switzerland, 2000.
[47] L.H. Han, Y.F. Yang, L. Xu, An experimental study and calculation on the fire resistance of concrete-filled SHS and RHS columns, J. Constr. Steel Res. 59 (4) (2003) 427-452.
[48] A. Espinos, M.L. Romero, E. Serra, A. Hospitaler, Circular and square slender concrete-filled tubular columns under large eccentricities and fire, J. Constr. Steel Res. 110 (2015) 90-100.
[49] A. Espinos, M.L. Romero, E. Serra, A. Hospitaler, Experimental investigation on the fire behaviour of rectangular and elliptical slender concrete-filled tubular columns, Thin-Walled Struct. 93 (2015) 137-148.
[50] V. Moliner, A. Espinos, M.L. Romero, A. Hospitaler, Fire behavior of eccentrically loaded slender high strength concrete-filled tubular columns, J. Constr. Steel Res. 83 (2013) 137-146.
[51] H. Yang, F.Q Liu, S.M. Zhang, X.T. Lv, Experimental investigation of concrete-filled square hollow section columns subjected to non-uniform exposure, Eng. Struct. 48 (2013) 292-312.
[52] H. Yang, F.Q. Liu, L. Gardner, Performance of concrete-filled RHS columns exposed to fire on 3 sides, Eng. Struct. 56 (2013) 1986-2004.
[53] ISO 834-1, Fire Resistance Test - Elements of Building Construction, Part 1: General Requirements, International Organization for Standardization ISO 834, Geneva, Switzerland, 1999.
[54] Lie TT, Chabot M. Experimental studies on the fire resistance of hollow steel columns filled with plain concrete. IRC Internal Report No. 611. Ottawa (Ontario): National Research Council of Canada, Institute for Research in Construction, 1992.
[55] Chabot M, Lie TT. Experimental studies on the fire resistance of hollow steel columns filled with bar-reinforced concrete. IRC Internal Report No. 628. Ottawa (Ontario): National Research Council of Canada, Institute for Research in Construction, 1992.
[56] Kodur VKR, Latour JC. Experimental studies on the fire resistance of hollow steel columns filled with high-strength concrete. IRC Internal Report No. 215. Ottawa (Ontario): National Research Council of Canada, Institute for Research in Construction, 2005.
[57] K. Wang, B. Young, Fire resistance of concrete-filled high strength steel tubular

columns, Thin-Walled Struct. 71 (2013) 46-56.
[58] M.X. Xiong, J.Y.R. Liew, Mechanical behaviour of ultra-high strength concrete at elevated temperatures and fire resistance of ultra-high strength concrete filled steel tubes, Mater. Design. 104 (2016) 414-427.
[59] F.Q. Liu, L. Gardner, H. Yang, Post-fire behaviour of reinforced concrete stub columns confined by circular steel tubes, J. Constr. Steel Res. 102 (2014) 82-103.
[60] H. Yang, F.Q. Liu, L. Gardner, Post-fire behaviour of slender reinforced concrete columns confined by circular steel tubes, Thin-Walled Struct. 87 (2015) 12-29.
[61] F.Q. Liu, H. Yang, L. Gardner, Post-fire behaviour of eccentrically loaded reinforced concrete columns confined by circular tubes, J. Constr. Steel Res. 122 (2016) 495-510.
[62] F.Q. Liu, H. Yang, R. Yan, W. Wang, Experimental and numerical study on behaviour of square steel tube confined reinforced concrete stub columns after fire exposure, Thin-Walled Struct. 139 (2019) 105-125.
[63] Wang X D. Study on the behavior and strength of TRC and TSRC columns. Doctoral dissertation, Harbin: Harbin Institute of Technology, 2017: 19-20. [in Chinese]
[64] ABAQUS 6.11-1 (Computer Software). Providence, RI: Dassault Systems Simulation Corporation; 2011.
[65] European Convention for Constructional Steelwork, Fire Safety of Steel Structures: Technical Note, Calculation of the Fire Resistance of Centrally Loaded Composite Steel-Concrete Columns Exposed to the Standard Fire vol. 3, ECCS Technical Committee, Brussels, Belgium, 1988.
[66] J. Ding, Y.C. Wang, Realistic modelling of thermal and structural behaviour of unprotected concrete filled tubular columns in fire, J. Constr. Steel Res. 64 (10) (2008) 1086-1102.
[67] L.H. Han, W.H. Wang, H.X. Yu, Analytical behaviour of RC beam to CFST column frames subjected to fire, Eng. Struct. 36 (2012) 394-410.
[68] L.H. Han, T.Y. Song, K. Zhou, Z.Q. Cui, Fire performance of CFST triple-limb laced columns, J. Struct. Eng. 144 (9) (2018) 04018157.
[69] Y.F. Yang, F. Fu, Fire resistance of steel beam to square CFST column composite joints using RC slabs: Experiments and numerical studies, Fire Safety J. 104 (2019) 90-108.
[70] L. Xu, Y.B. Liu, Concrete filled steel tube reinforced concrete (CFSTRC) columns

subjected to ISO-834 standard fire: experiment, Adv. Struct. Eng. 16 (7) (2013) 1263-1282.

[71] E.F. Du, G.P. Shu, X.Y. Mao, Analytical behavior of eccentrically loaded concrete encased steel columns subjected to standard fire including cooling phase, Int. J. Steel Struct. 13 (1) (2013) 129-140.

[72] EN 1991-1-2, Eurocode 1 - Actions on Structures - Part 1-2: General Actions - Actions on Structures Exposed to Fire, CEN, Brussels, 2002.

[73] ASCE 1992. Structural fire protection. Manual of Practice No. 78. Reston, VA: ASCE.

[74] EN 1992-1-2, Eurocode 2 - Design of Concrete Structures - Part 1-2: General Rules - Structural Fire Design, CEN, Brussels, 2004.

[75] T.T. Lie, Fire resistance of circular steel columns filled with bar-reinforced concrete, J. Struct. Eng. 120 (5) (1994) 1489-1509.

[76] X.T. Lv, H. Yang, S.M. Zhang, Effect of contact thermal resistance on temperature distributions of concrete-filled steel tubes in fire, J Harbin Inst Technol. 18 (1) (2011) 81-88.

[77] T. Gernay, A. Millard, J.M. Franssen, A multiaxial constitutive model for concrete in the fire situation: theoretical formulation, Int. J. Solids Struct. 50 (22-23) (2013) 3659-3673.

[78] EN 1993-1-2, Eurocode 3 - Design of Steel Structures - Part 1-2: General Rules - Structural Fire Design, CEN, Brussels, 2005.

[79] A. Espinos, M.L. Romero, A. Hospitaler, Advanced model for predicting the fire response of concrete filled tubular columns, J. Constr. Steel Res. 66 (8-9) (2010) 1030-1046.

[80] M. Neuenschwander, M. Knobloch, M. Fontana, Modeling thermo-mechanical behavior of concrete-filled steel tube columns with solid steel core subjected to fire, Eng. Struct. 136 (2017) 180-193.

[81] L.H. Han, X.L. Zhao, Y.F. Yang, J.B. Feng, Experimental study and calculation of fire resistance of concrete-filled hollow steel columns, J. Struct. Eng. 129 (3) (2003) 346-356.

List of Figures

Fig. 1 Schematics of TRC column and TRC column-RC beam connection (a) TRC column; (b) TRC column-RC beam connection.

Fig. 2 Drawings of the tested square TRC columns (unit: mm) (a) 2D and 3D schematic diagrams; (b) Cross-section details; (c) Arrangement of thermocouples.

Fig. 3 Test procedure, loading precision, furnace temperature and axial deformation of specimen TRC-0.4-0 (a) Test procedure; (b) Loading precision; (c) Furnace temperature; (d) Axial deformation.

Fig. 4 Test setup and details (unit: mm) (a) Sketch of the test setup; (b) Photo of the test setup; (c) Sketch of top loading device; (d) Photo of top loading device; (e) Sketch of bottom loading device.

Fig. 5 Failure modes and residual deformations of tested square TRC slender columns (a) TRC-0.4-0; (b) TRC-0.5-0; (c) TRC-0.6-0; (d) TRC-0.5-25; (e) TRC-0.5-50; (f) Details of the gaps (TRC-0.4-0).

Fig. 6 Photos of specimens TRC-0.5-25 and TRC-0.6-0 after fire tests (a) Overall view (TRC-0.5-25); (b) Concrete crushing and re-bar buckling in compression zone (TRC-0.5-25); (c) Concrete cracks in tension zone (TRC-0.5-25); (d) Overall view (TRC-0.6-0); (e) Concrete crushing (TRC-0.6-0); (f) Re-bar buckling (TRC-0.6-0).

Fig. 7 Furnace air temperatures and uniformity of the temperature fields within the tested specimens (a) Furnace air temperature; (b) Points 1, 6; (c) Points 7, 10; (d) Points 8, 9; (e) Point 2; (f) Point 3; (g) Point 4; (h) Point 5.

Fig. 8 Axial and lateral deformation-time relationships of tested TRC columns (a) TRC-0.4-0; (b) TRC-0.5-0; (c) TRC-0.6-0; (d) TRC-0.5-25; (e) TRC-0.5-50.

Fig. 9 Influences of load ratio and load eccentricity on the fire performance of test specimens (a) Axial deformation vs load ratio; (b) Lateral deformation vs load ratio; (c) Endplate rotation vs load ratio; (d) Fire resistance & Limiting temperature vs load ratio; (e) Axial deformation vs load eccentricity; (f) Lateral deformation vs load eccentricity; (g) Endplate rotation vs load eccentricity; (h) Fire resistance & Limiting temperature vs load eccentricity.

Fig. 10 Comparison of the temperature-time curves given by FEA modelling and experiments conducted in this study (a) Points 1, 6 (TRC-0.4-0); (b) Points 7, 10 (TRC-0.4-0); (c) Points 8, 9 (TRC-0.4-0); (d) Point 2 (TRC-0.4-0); (e) Point 5 (TRC-0.4-0); (f) Points 1, 6 (TRC-0.5-0); (g) Points 7, 10 (TRC-0.5-0); (h) Points 8, 9 (TRC-0.5-0); (i) Point 2 (TRC-0.5-0); (j) Point 5 (TRC-0.5-0); (k) Points 1, 6 (TRC-0.6-0); (l) Points 7, 10 (TRC-0.6-0); (m) Points 8, 9 (TRC-0.6-0); (n) Point 2 (TRC-0.6-0); (o) Point 5 (TRC-0.6-0); (p) Points 1, 6

List of Tables

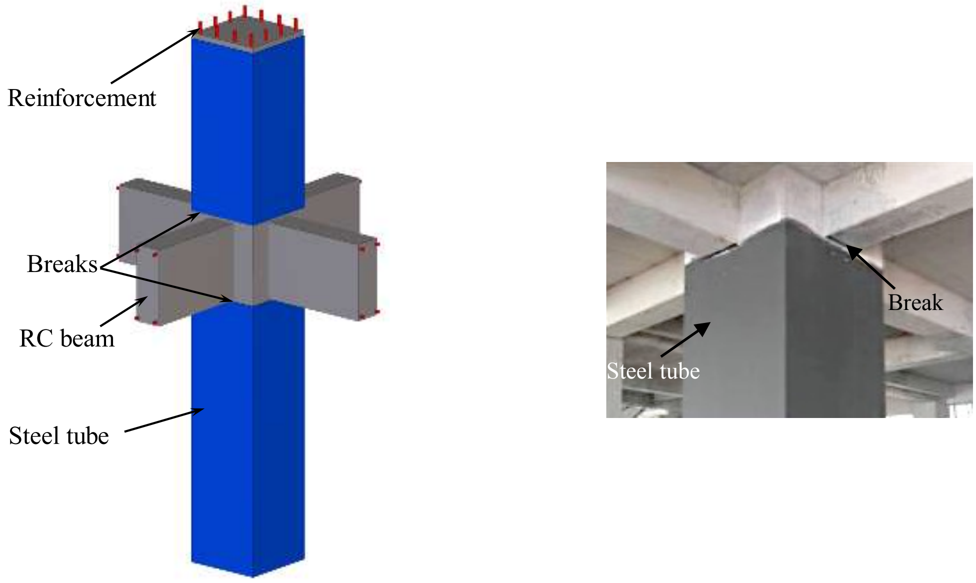

(a) TRC column (b) TRC column-RC beam connection

Fig. 1. Schematics of TRC column and TRC column-RC beam connection

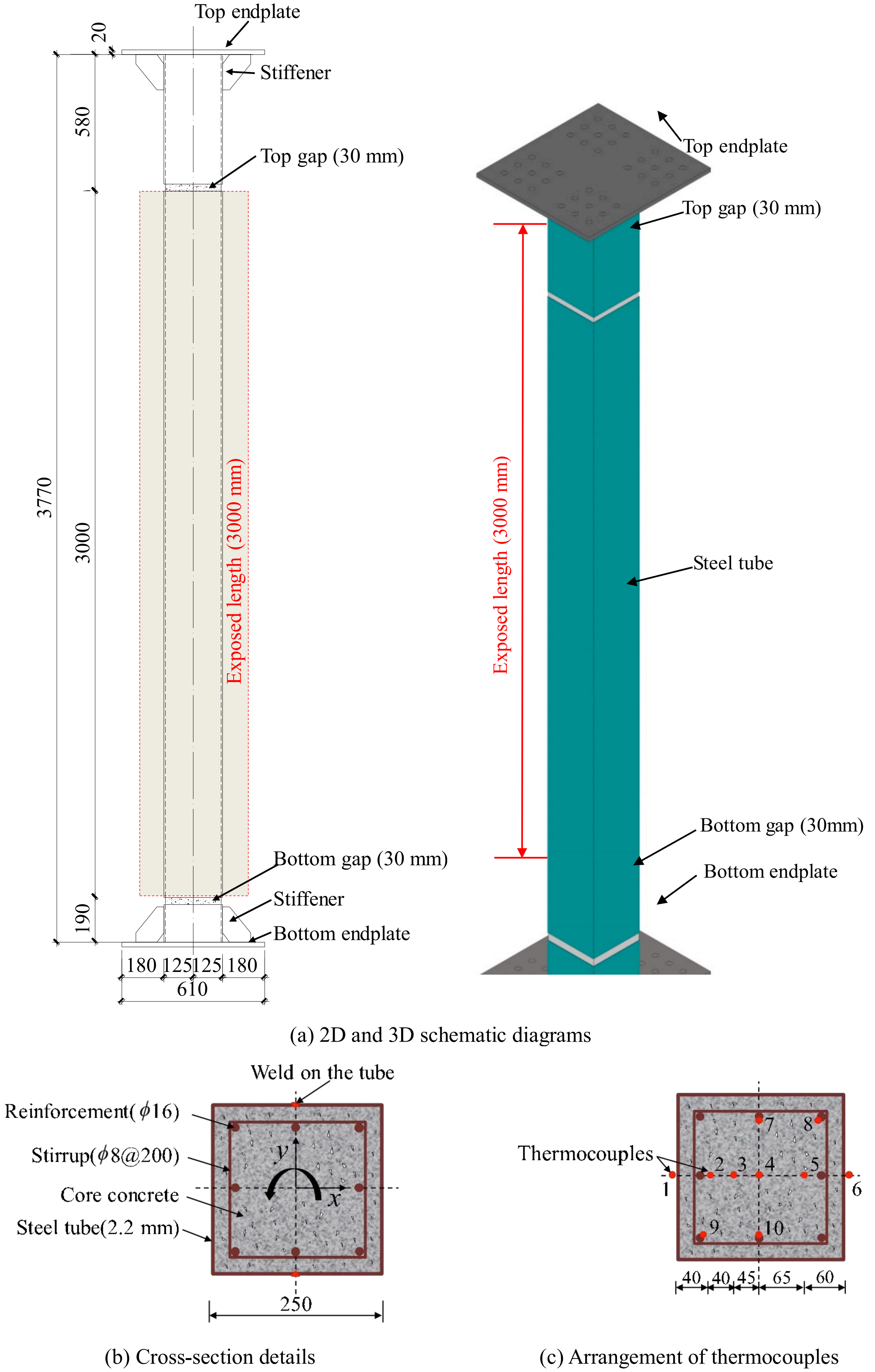

Fig. 2. Drawings of the tested square TRC columns (unit: mm)

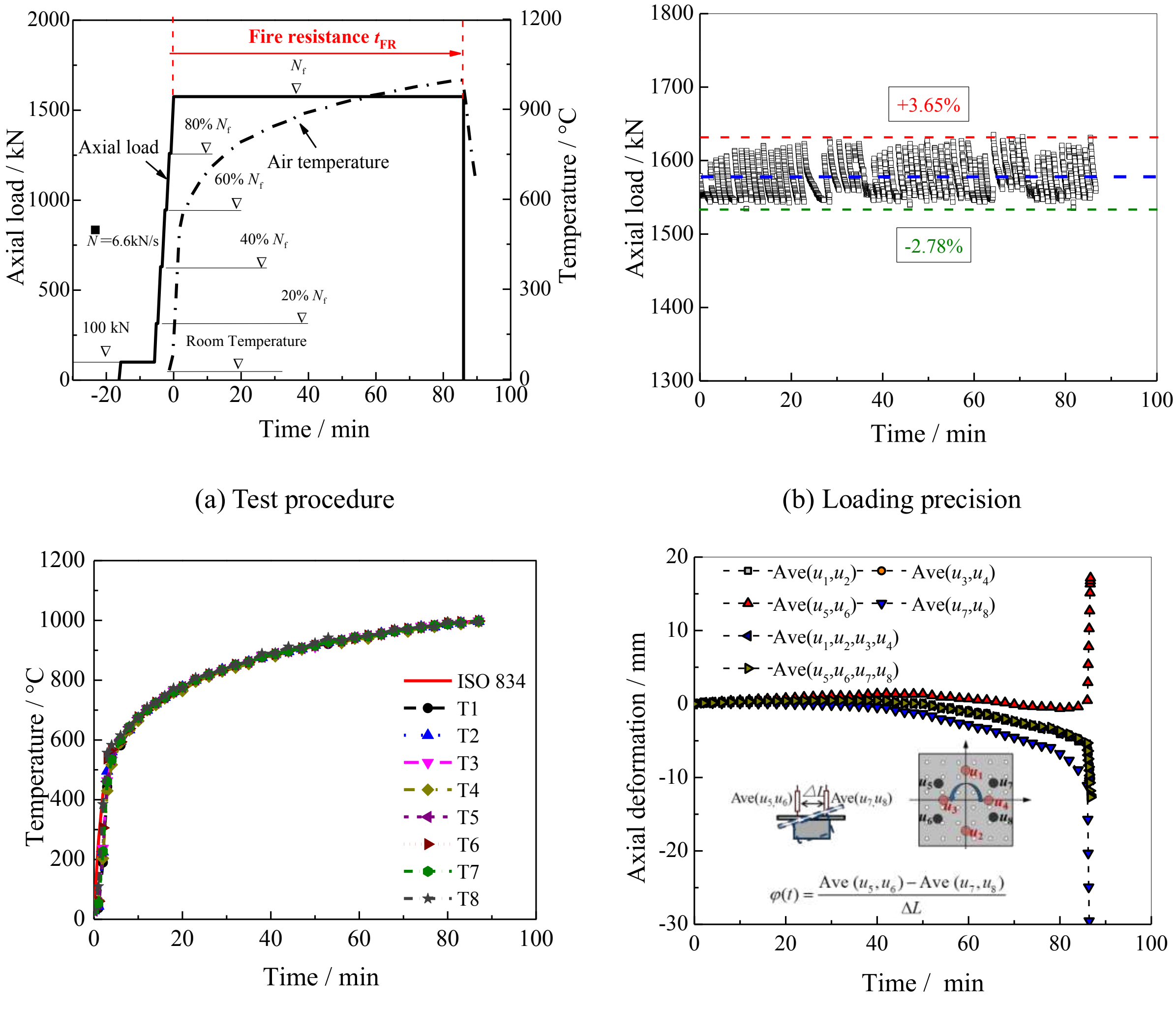

(a) Test procedure

(b) Loading precision

(c) Furnace temperature

(d) Axial deformation

Fig. 3. Test procedure, loading precision, furnace temperature and axial deformation of specimen TRC-0.4-0

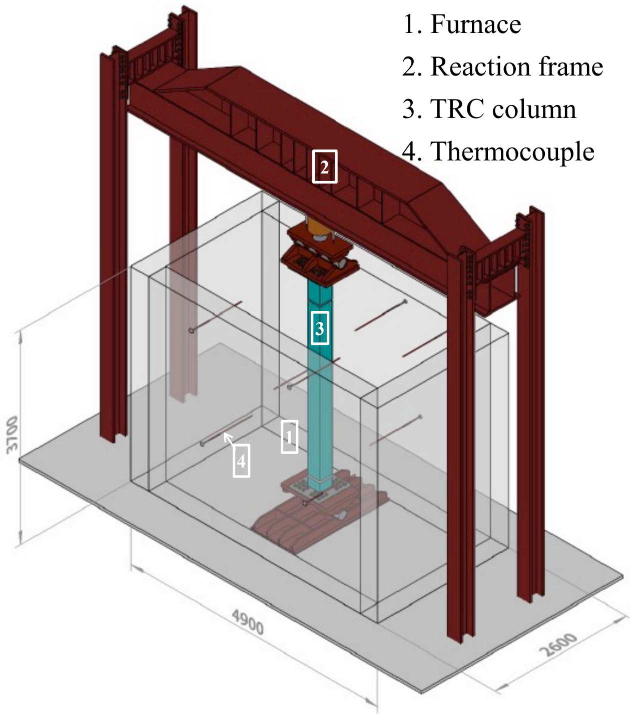

(a) Sketch of the test setup

(b) Photo of the test setup

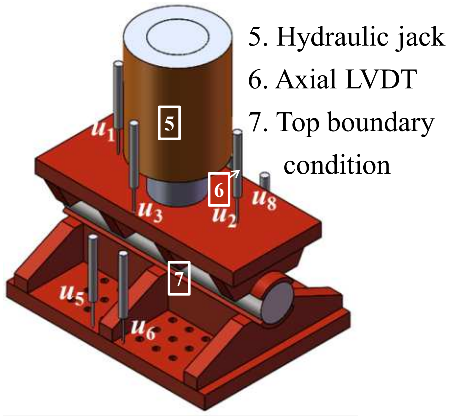

(c) Sketch of top loading device

(d) Photo of top loading device

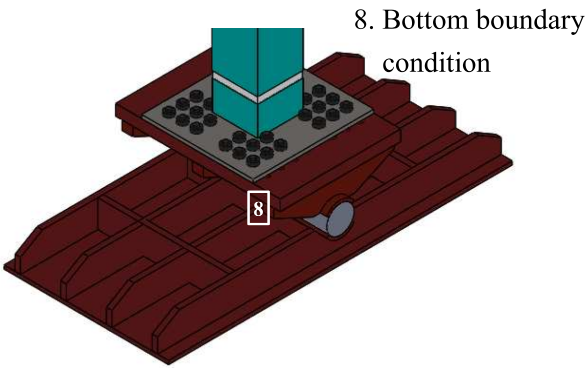

(e) Sketch of bottom loading device

Fig. 4. Test setup and details (unit: mm)

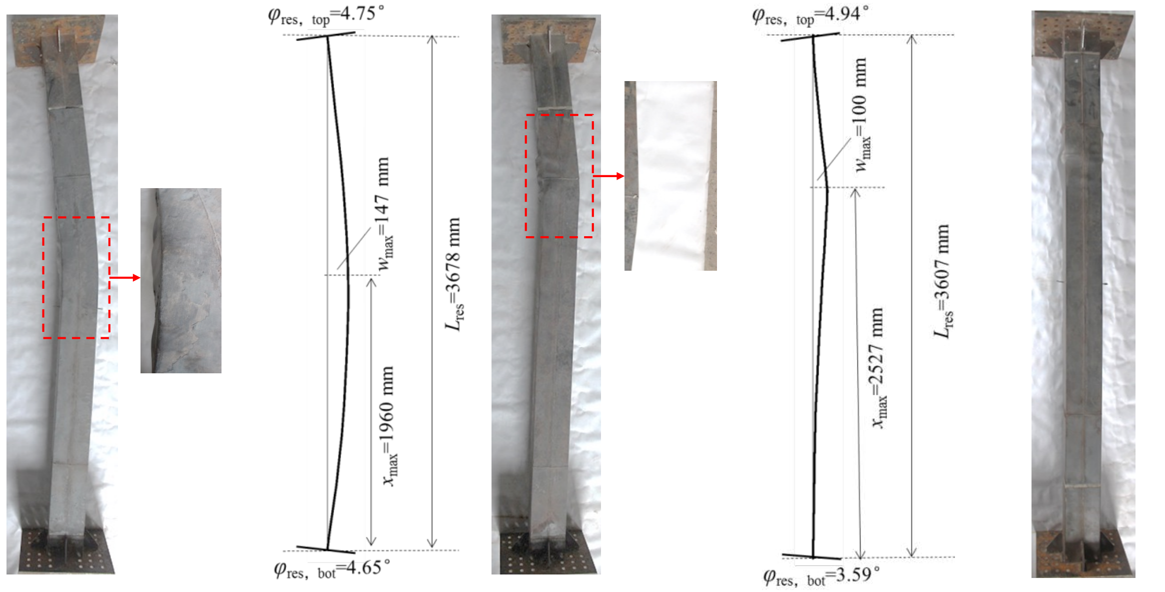

(a) TRC-0.4-0 (b) TRC-0.5-0 (c) TRC-0.6-0

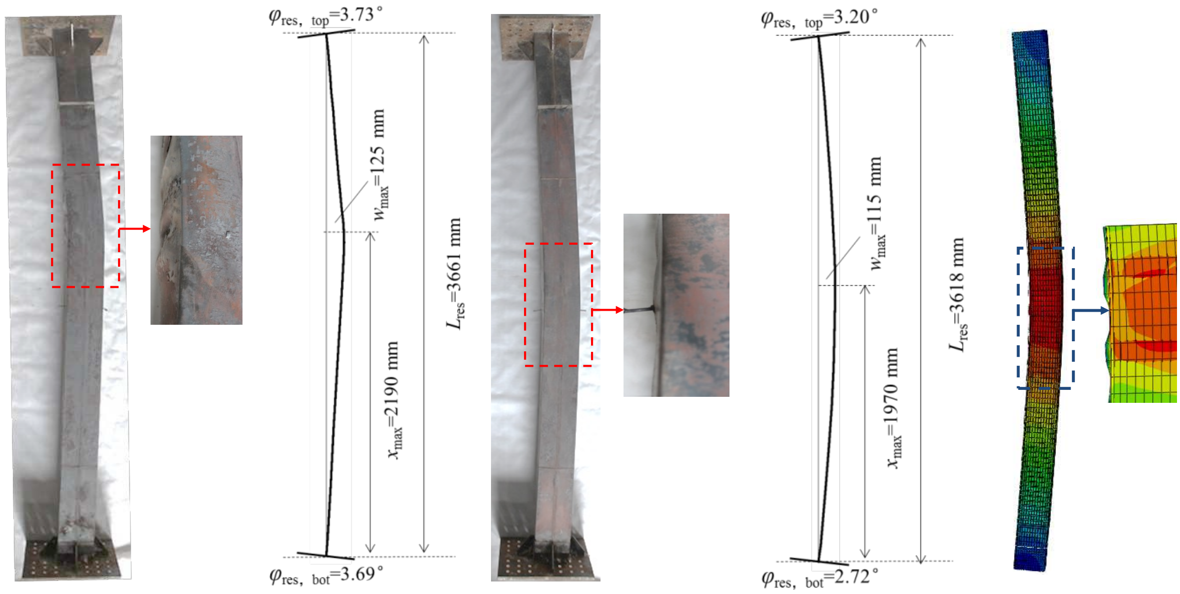

(d) TRC-0.5-25 (e) TRC-0.5-50

(f) Details of the gaps (TRC-0.4-0)

Fig. 5. Failure modes and residual deformations of tested square TRC slender columns

(a) Overall view (TRC-0.5-25)

(b) Concrete crushing and re-bar buckling in compression zone (TRC-0.5-25)

(c) Concrete cracks in tension zone (TRC-0.5-25)

(d) Overall view (TRC-0.6-0)

(e) Concrete crushing (TRC-0.6-0)

(f) Re-bar buckling (TRC-0.6-0)

Fig. 6. Photos of specimens TRC-0.5-25 and TRC-0.6-0 after fire tests

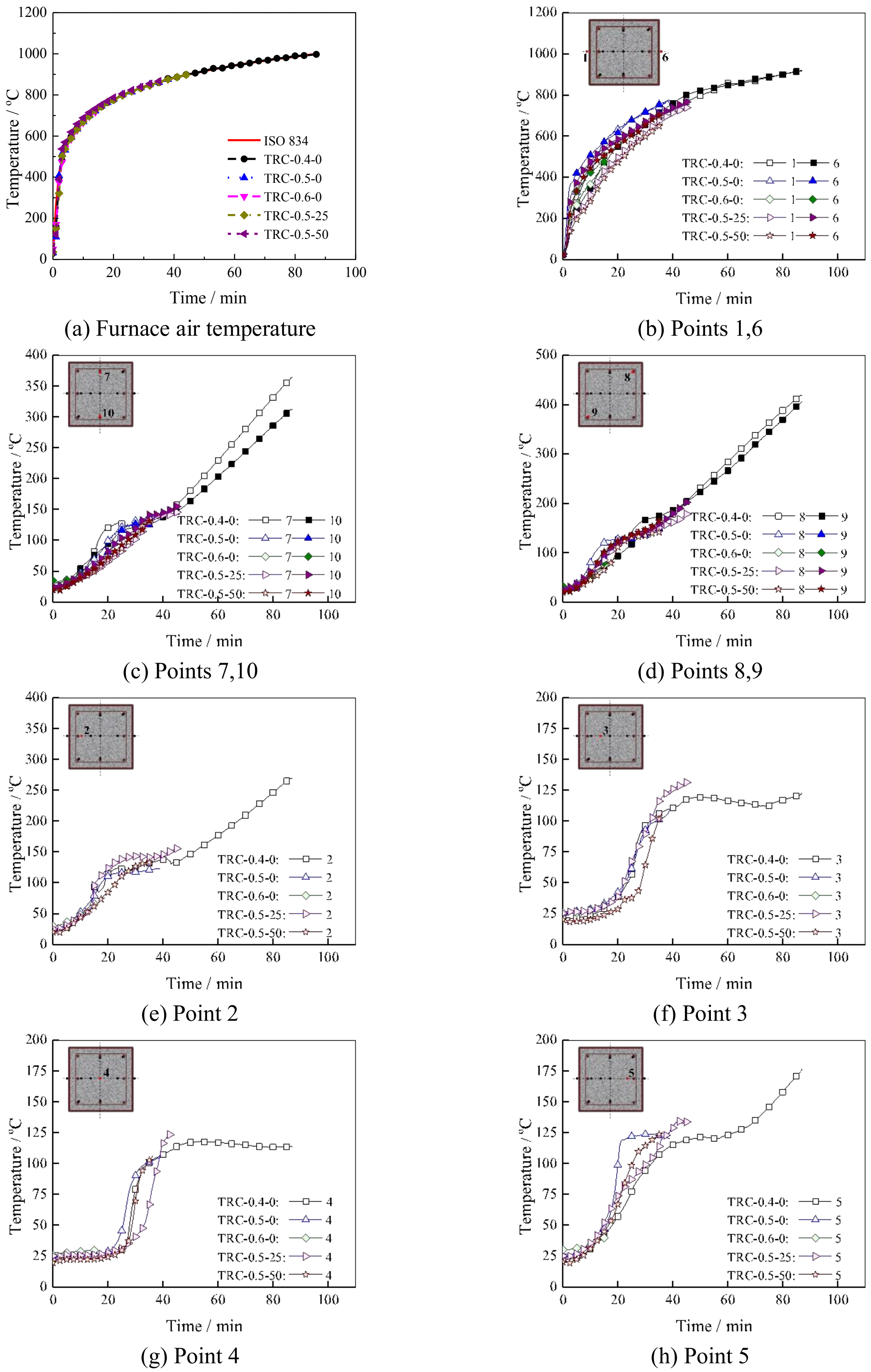

(a) Furnace air temperature
(b) Points 1,6
(c) Points 7,10
(d) Points 8,9
(e) Point 2
(f) Point 3
(g) Point 4
(h) Point 5

Fig. 7. Furnace air temperatures and uniformity of the temperature fields within the tested specimens

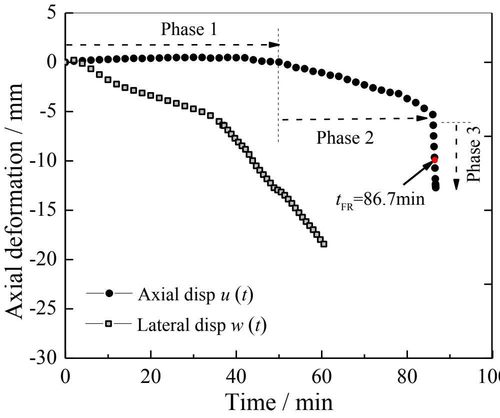

(a) TRC-0.4-0

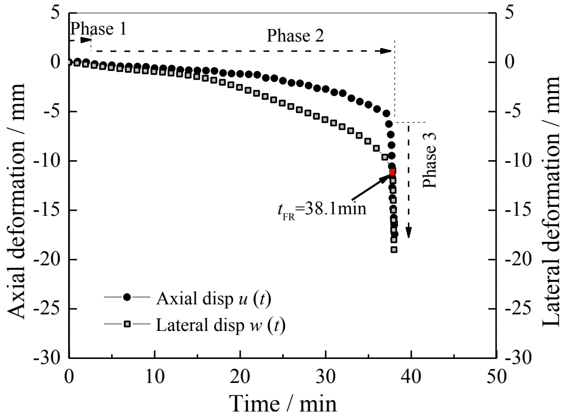

(b) TRC-0.5-0

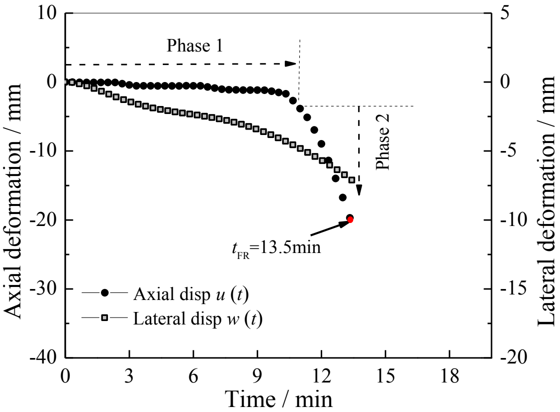

(c) TRC-0.6-0

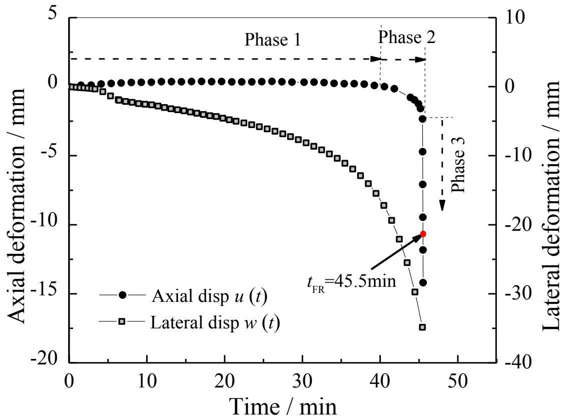

(d) TRC-0.5-25

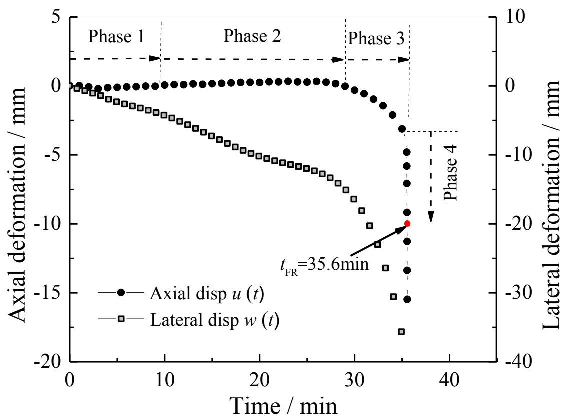

(e) TRC-0.5-50

Fig. 8. Axial and lateral deformation-time relationships of tested TRC columns

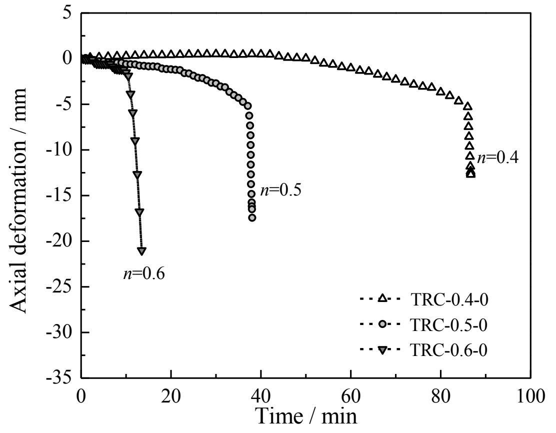

(a) Axial deformation vs load ratio

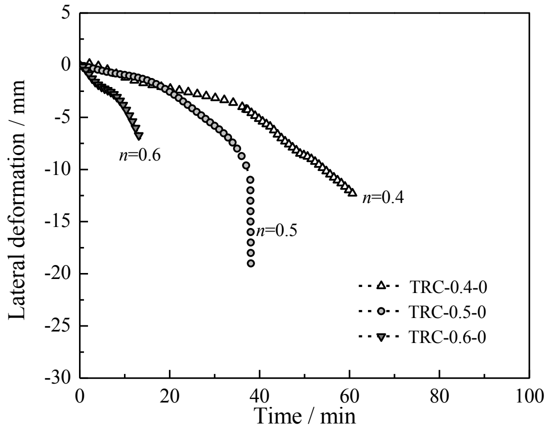

(b) Lateral deformation vs load ratio

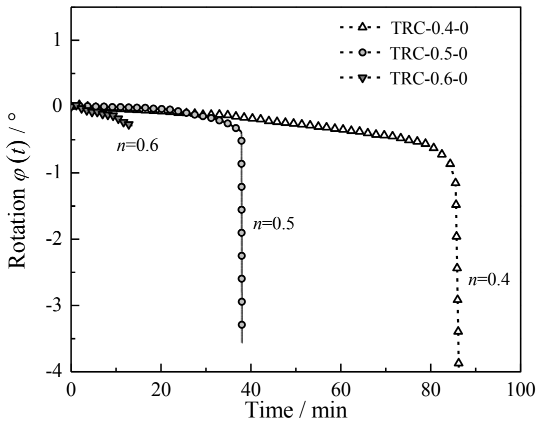

(c) Endplate rotation vs load ratio

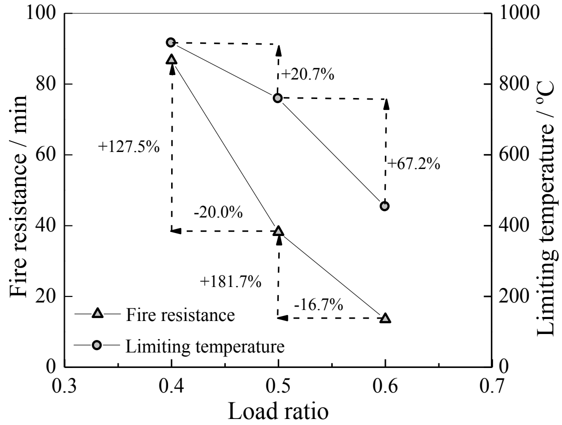

(d) Fire resistance & Limiting temperature vs load ratio

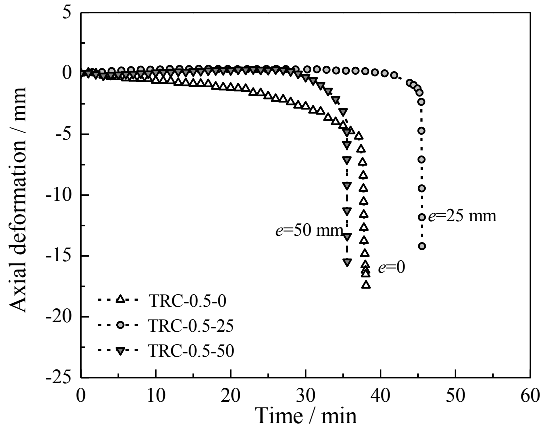

(e) Axial deformation vs load eccentricity

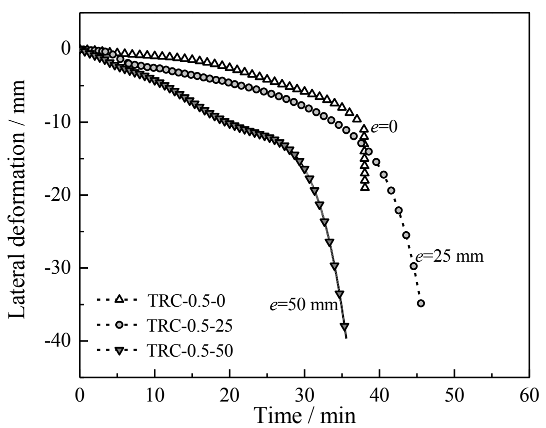

(f) Lateral deformation vs load eccentricity

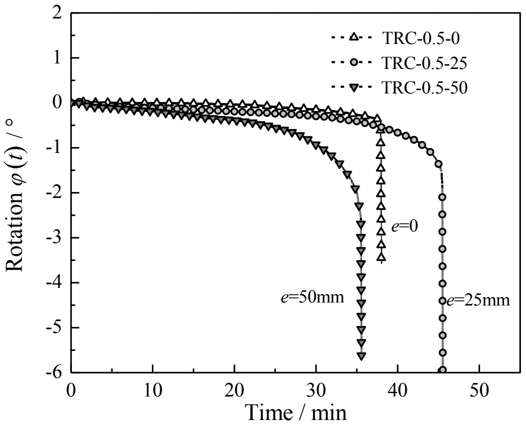

(g) Endplate rotation vs load eccentricity

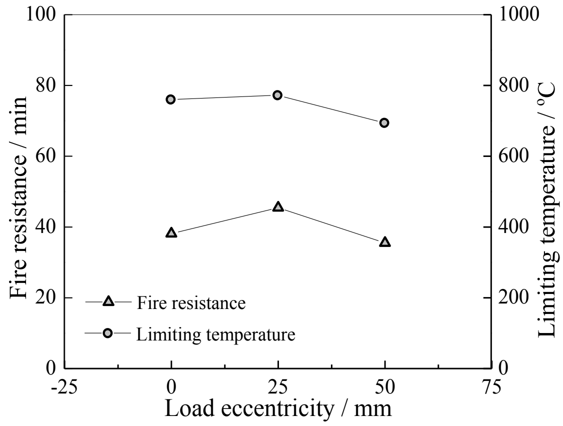

(h) Fire resistance & Limiting temperature vs load eccentricity

Fig. 9. Influences of load ratio and load eccentricity on the fire performance of test specimens

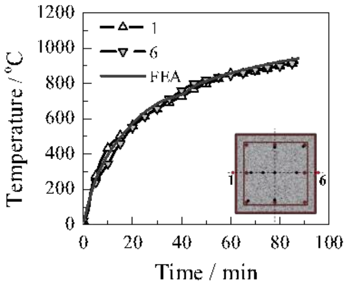

(a) Points 1,6 (TRC-0.4-0)

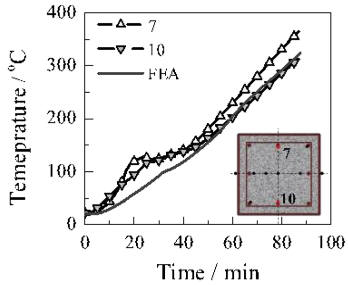

(b) Points 7,10 (TRC-0.4-0)

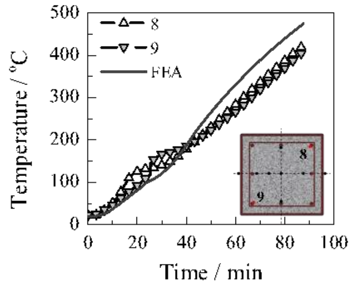

(c) Points 8,9 (TRC-0.4-0)

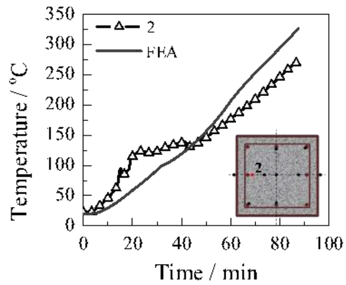

(d) Point 2 (TRC-0.4-0)

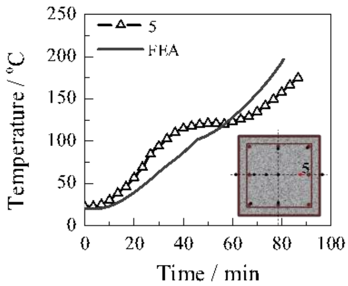

(e) Point 5 (TRC-0.4-0)

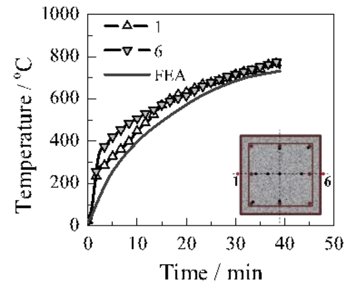

(f) Points 1,6 (TRC-0.5-0)

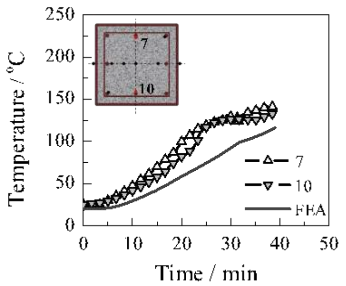

(g) Points 7,10 (TRC-0.5-0)

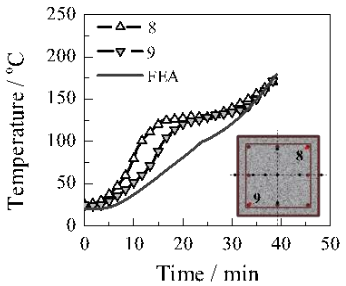

(h) Points 8,9 (TRC-0.5-0)

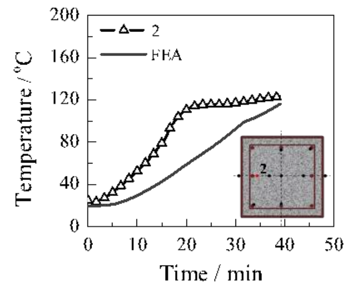

(i) Point 2 (TRC-0.5-0)

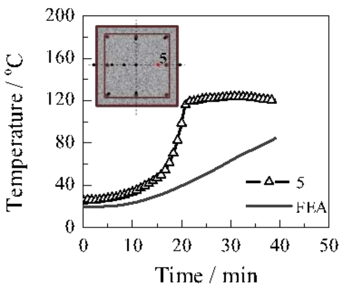

(j) Point 5 (TRC-0.5-0)

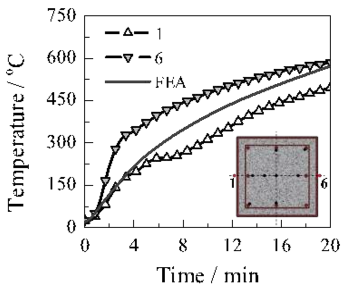

(k) Points 1,6 (TRC-0.6-0)

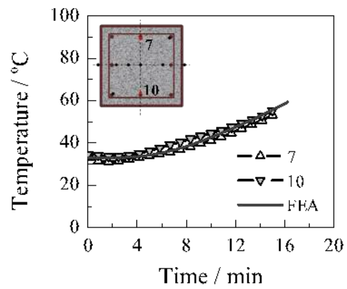

(l) Points 7,10 (TRC-0.6-0)

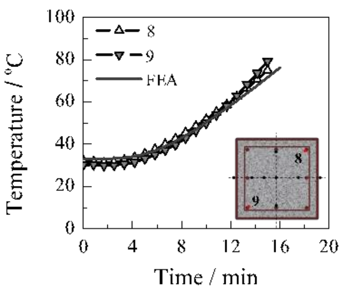

(m) Points 8,9 (TRC-0.6-0)

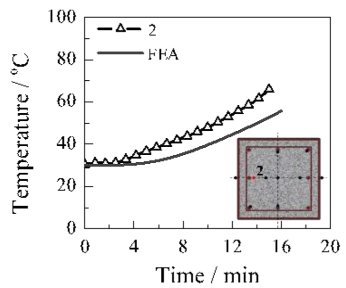

(n) Point 2 (TRC-0.6-0)

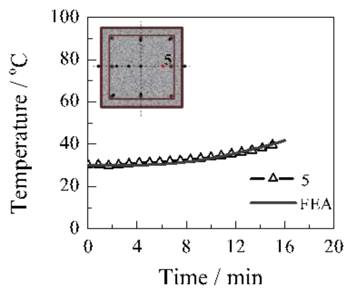

(o) Point 5 (TRC-0.6-0)

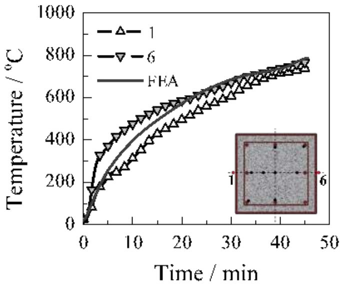

(p) Points 1,6 (TRC-0.5-25)

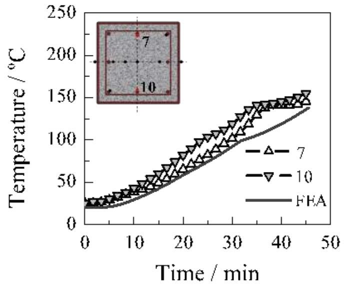

(q) Points 7,10 (TRC-0.5-25)

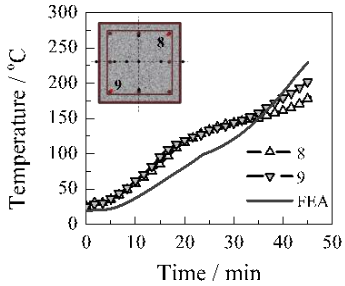

(r) Points 8,9 (TRC-0.5-25)

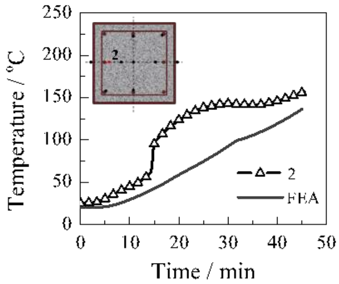

(s) Point 2 (TRC-0.5-25)

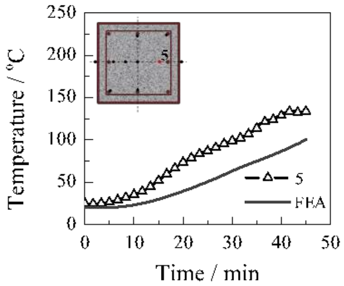

(t) Point 5 (TRC-0.5-25)

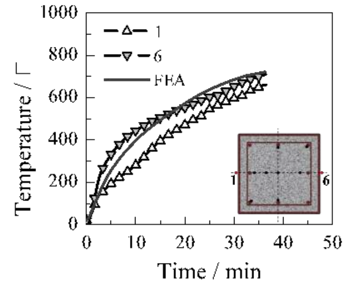

(u) Points 1,6 (TRC-0.5-50)

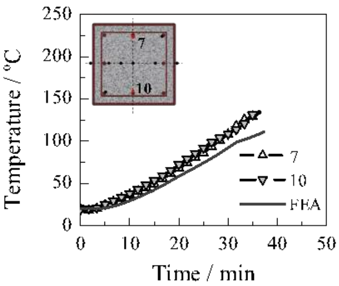

(v) Points 7,10 (TRC-0.5-50)

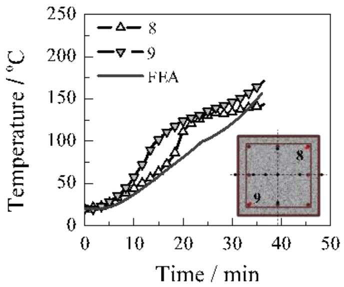

(w) Points 8,9 (TRC-0.5-50)

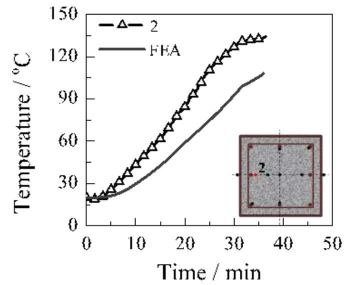

(x) Point 2 (TRC-0.5-50)

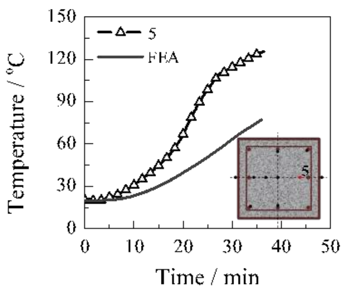

(y) Point 5 (TRC-0.5-50)

Fig. 10. Comparison of the temperature-time curves given by FEA modelling and experiments conducted in this study

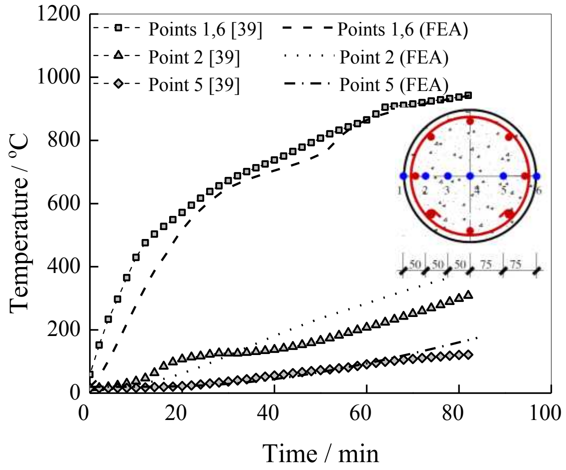

(a) Temperature (STCRC-2)

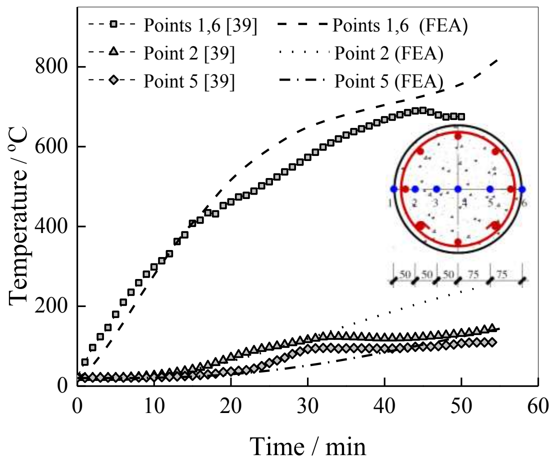

(b) Temperature (STCRC-3)

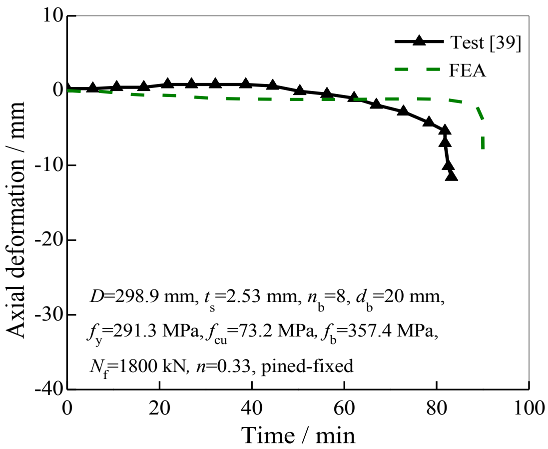

(c) Axial deformation (STCRC-2)

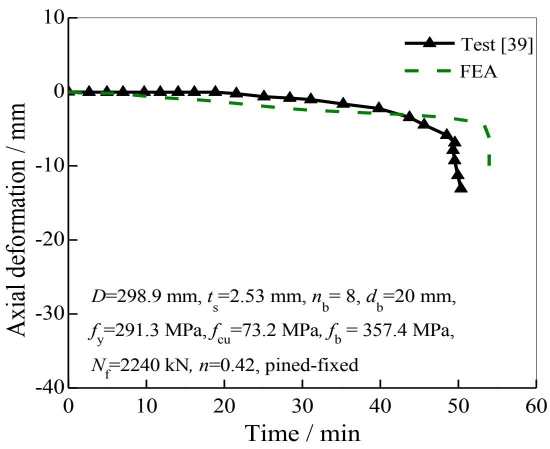

(d) Axial deformation (STCRC-3)

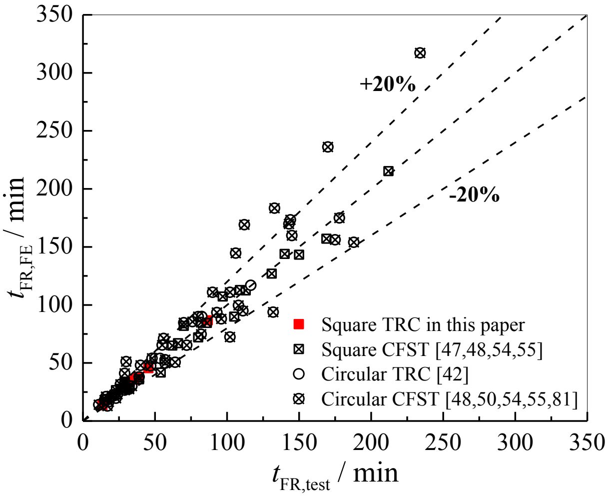

(e) Fire resistance of composite columns

Fig. 11. Validation of the FEA modelling against the experimental results of circular TRC columns and CFST columns conducted by other researchers

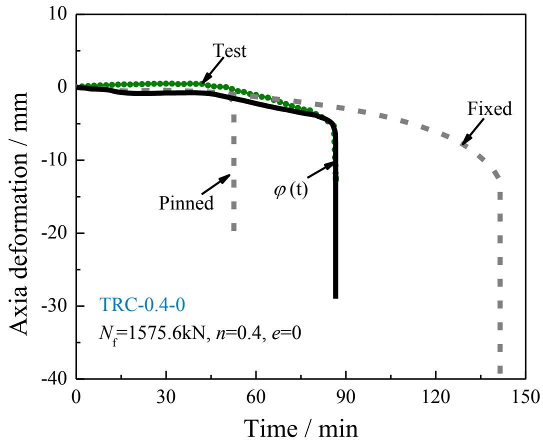

(a) Axial deformation (TRC-0.4-0)

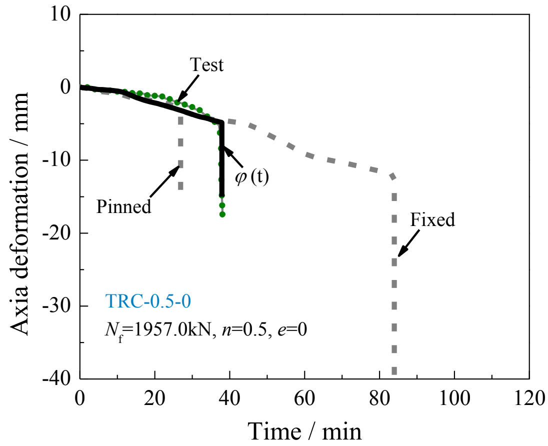

(b) Axial deformation (TRC-0.5-0)

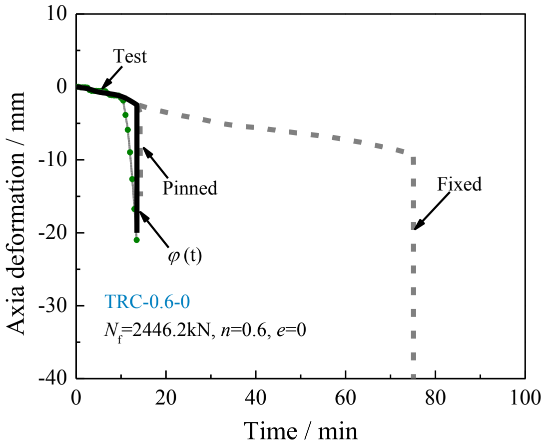

(c) Axial deformation (TRC-0.6-0)

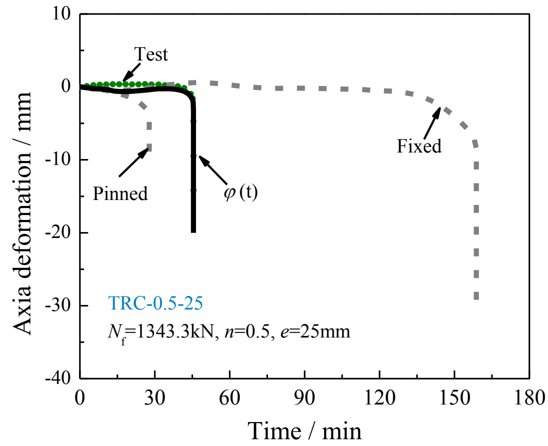

(d) Axial deformation (TRC-0.5-25)

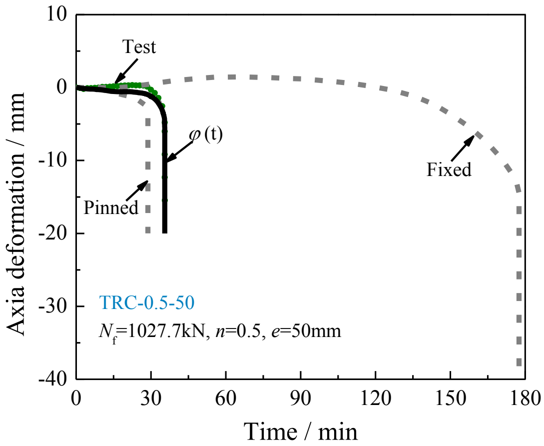

(e) Axial deformation (TRC-0.5-50)

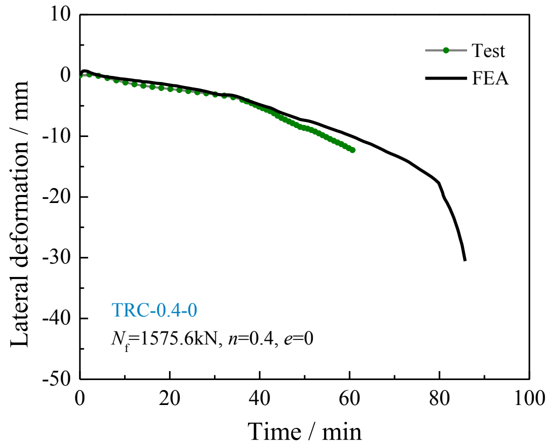

(f) Lateral deformation (TRC-0.4-0)

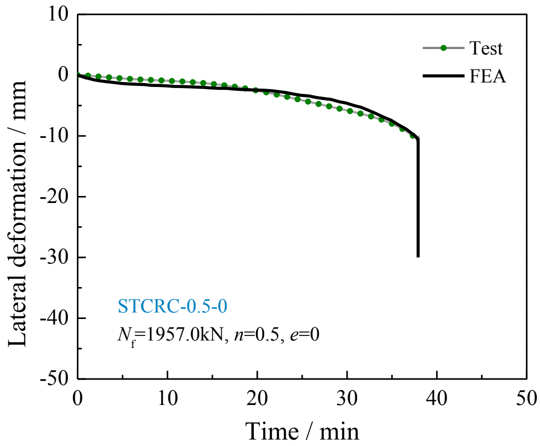

(g) Lateral deformation (TRC-0.5-0)

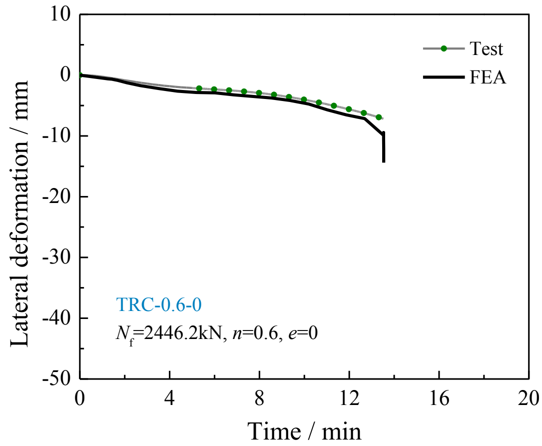

(h) Lateral deformation (TRC-0.6-0)

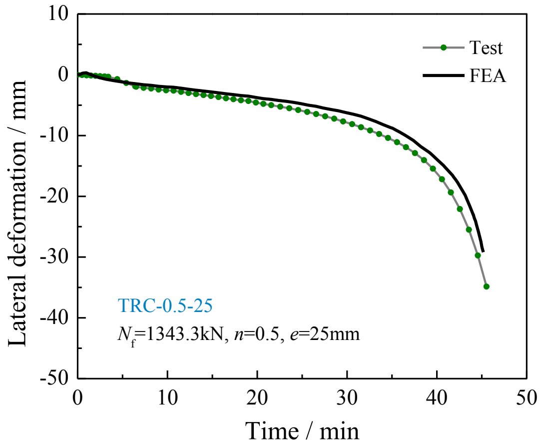

(i) Lateral deformation (TRC-0.5-25)

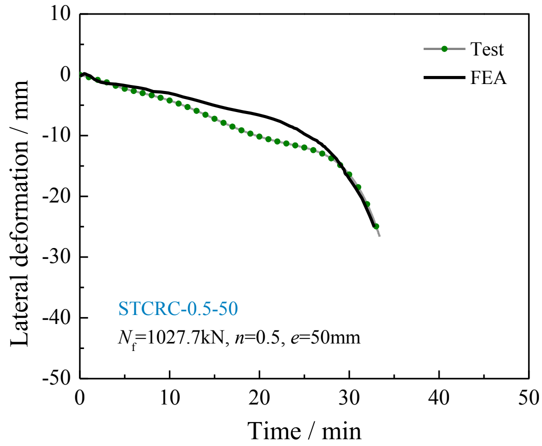

(j) Lateral deformation (TRC-0.5-50)

Fig. 12. Axial and lateral deformation-time curves given by the FEA modelling vs experiments conducted in this study

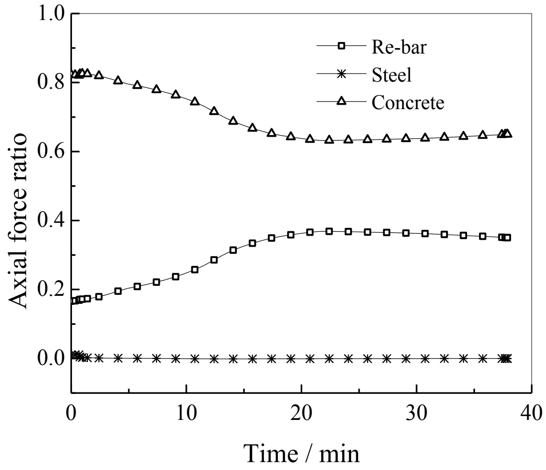

(a) Axial force ratios

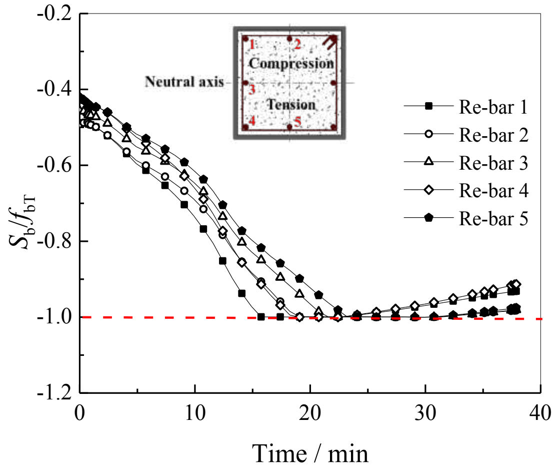

(b) Normalized stress-time curves of re-bars

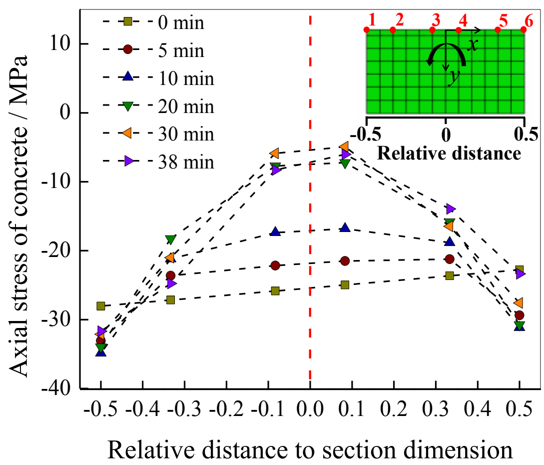

(c) Axial stress distribution of concrete nodes

Fig. 13. Load redistribution and stress evolutions of column TRC-0.5-0

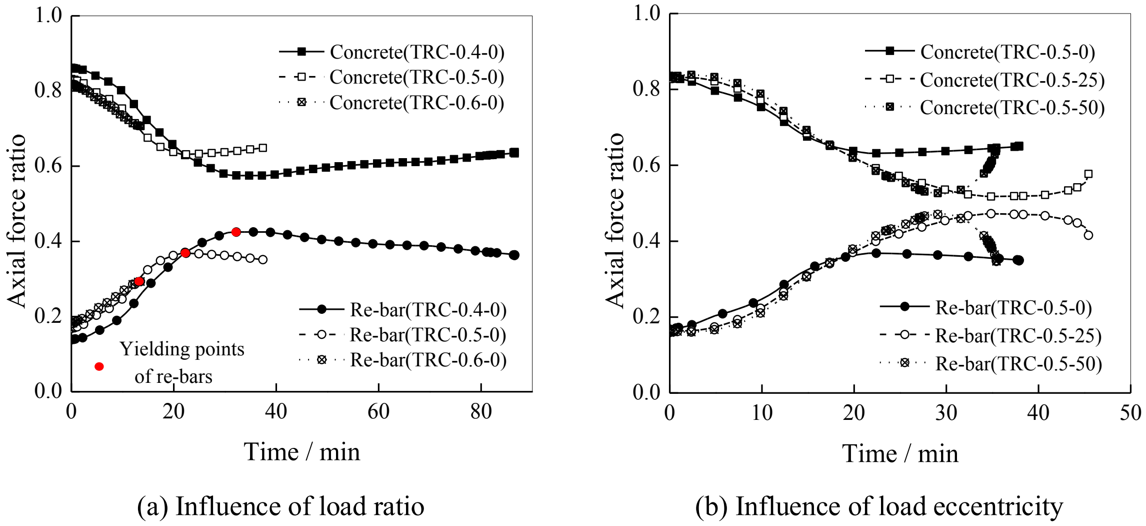

Fig. 14. Load redistribution for the tested square TRC columns

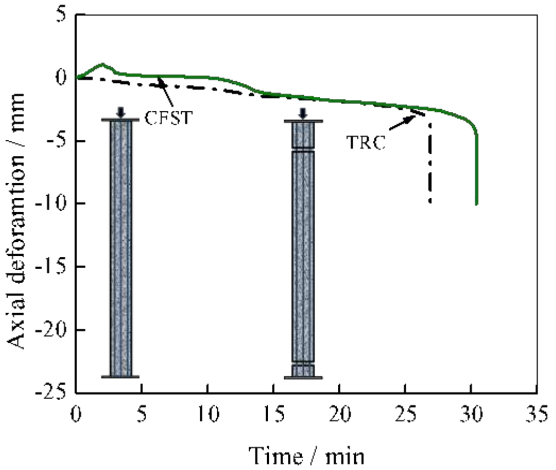

(a) Axial deformation (D=250 mm)

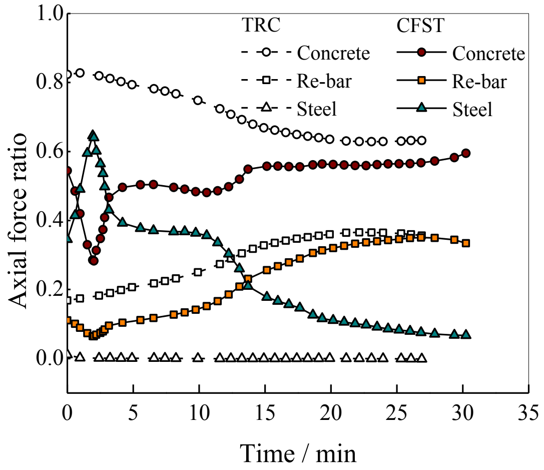

(b) Load redistribution (D=250 mm)

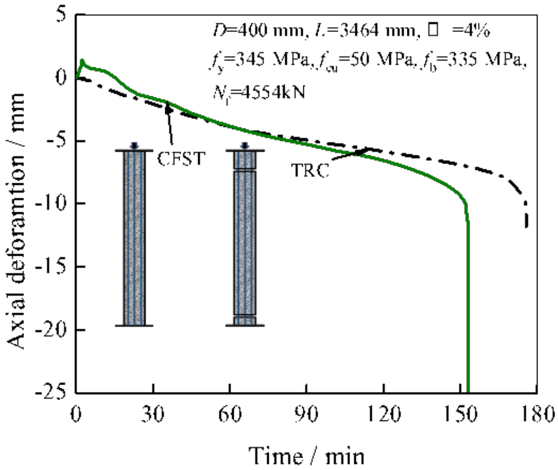

(c) Axial deformation (D=400 mm)

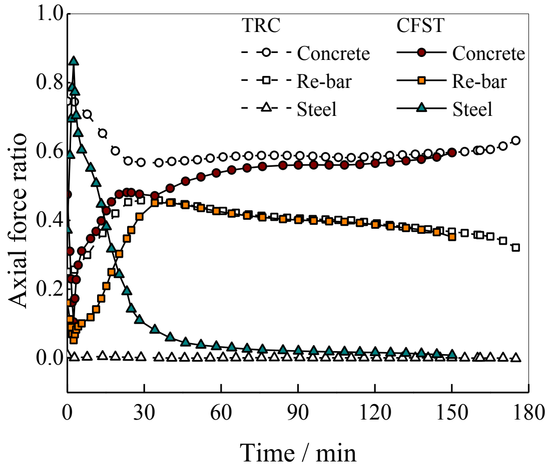

(d) Load redistribution (D=400 mm)

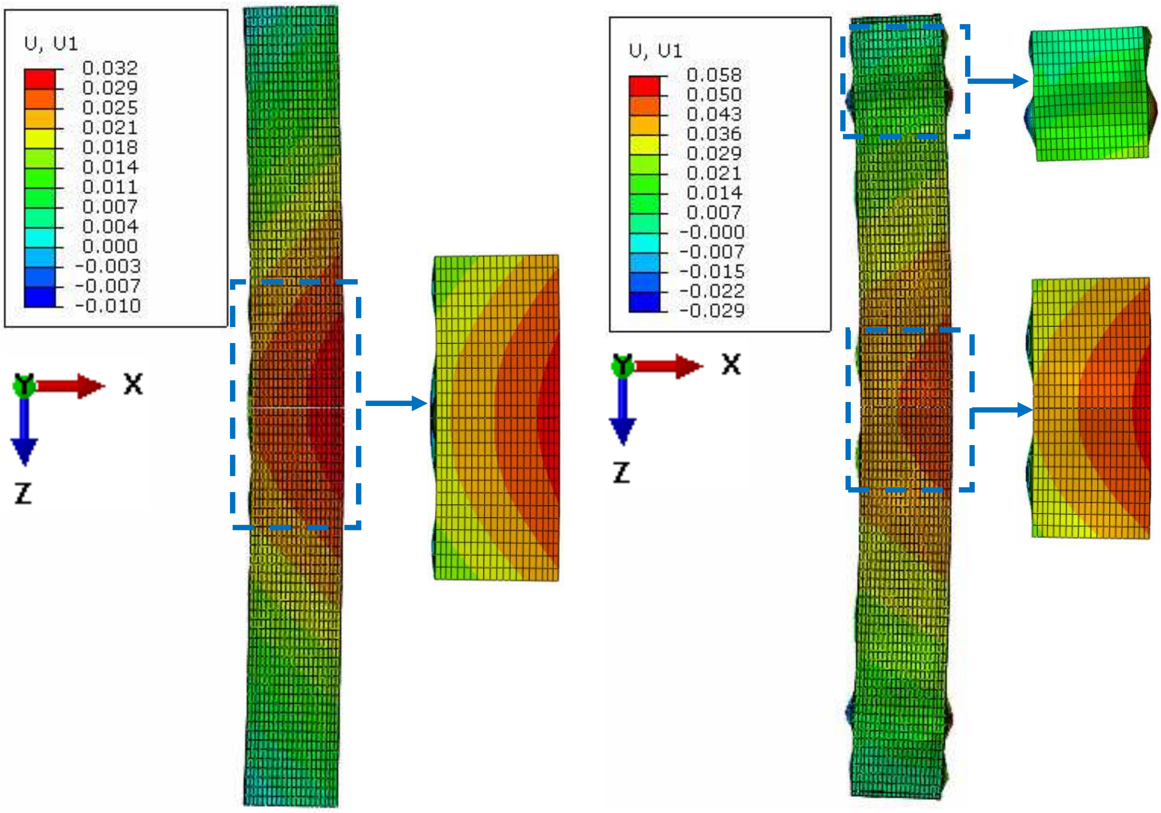

(e) Failure mode of the TRC (*D*=400 mm)　　　　(f) Failure mode the CFST (*D*=400 mm)

Fig. 15. Comparison of the fire behaviour between the TRC columns and the CFST columns

Table 1

Typical engineering applications of TRC columns in China

Name	Type	Year	Height or Span (m)	Section shape and dimension (mm)
Harbin Investment Mansion	High-rise building	2010	170	Square (1200 & 1300)
Harbin Technology & Innovation Mansion	High-rise building	2011	200	Square (900)
Dalian PetroChina Mansion	High-rise building	2011	176	Rectangular (900×700 oblique column) (1400×1100 vertical column)
China Resources Xiaojing Bay Hotel	High-rise building	2016	44.6	Rectangular (n.a.)
Qingdao Haitian Centre	High-rise building	2018	210 (T1) 245 (T3)	Circular (1400 & 1500)
Heixiazi Island Dongji Pagoda	Pagoda	2012	81	Circular (1200)
Dalian Gymnasium	Large-span gymnasium	2010	116×140	Rectangular (1800×1000) Circular (1500)
Dandong Olympic Stadium	Large-span stadium	2011	256×288	Circular (1200)
Dalian Stadium	Large-span stadium	2012	320×293	Rectangular (1000×800) Circular (1200)

Table 2

Details of the tested square TRC columns

Specimen name	D×B (mm)		t_s (mm)		L (mm)	α (%)	ρ (%)	e (mm)	n	N_f (kN)	t_{FR} (min)
	Nominal	Measured	Nominal	Measured							
TRC-0.4-0	250×250	251.3×250.6	2.2	2.19	3810	3.62	2.67	0	0.4	1575.6	86.7
TRC-0.5-0	250×250	251.9×251.5	2.2	2.17	3810	3.62	2.67	0	0.5	1957.1	38.1
TRC-0.6-0	250×250	251.7×251.4	2.2	2.21	3810	3.62	2.67	0	0.6	2446.2	13.5
TRC-0.5-25	250×250	251.3×250.6	2.2	2.18	3810	3.62	2.67	25	0.5	1343.3	45.5
TRC-0.5-50	250×250	252.1×250.7	2.2	2.19	3810	3.62	2.67	50	0.5	1027.7	35.6

Table 3

Mechanical properties of steel tube and re-bars at ambient temperature

	ϕ or t_s (mm)	f_y or f_b (MPa)	f_u (MPa)	E_s (10^5MPa)	v	ε_f (%)
Re-bar-16	15.65	441.33	626.41	2.05	0.29	17.71
Stirrup-10	9.87	361.00	574.96	2.09	0.30	19.61
Stirrup-8	7.95	343.25	562.17	2.04	0.30	25.63
Steel tube	2.18	280.72	442.94	2.06	0.30	40.83

Table 4

Mix proportions and mechanical properties of the SCC

Cement (kg/m^3)	Mineral powder (kg/m^3)	Fly ash (kg/m^3)	Expanding agent (kg/m^3)	Medium sand (kg/m^3)	Coarse aggregate (kg/m^3)	Water (kg/m^3)	Superplasticizer (kg/m^3)	$f_{cu,28}$ (MPa)	$f_{cu,test}$ (MPa)	$E_{c,28}$ (10^4MPa)	$E_{c,test}$ (10^4MPa)	Moisture content (%)	Concrete age (day)
210	100	100	40	800	900	185	11	31.53	50.95	2.81	3.88	5.4	190

Table 5

Details of the fire tests of TRC and CFST columns

Reference	Column Type	Column No.	D (mm)	t_s (mm)	L (m)	Re-bars	e (mm)	f_y (MPa)	f_c' (MPa)	f_b (MPa)	N_f (kN)	$t_{FR,test}$ (min)	$t_{FR,FE}$ (min)	$t_{FR,FE}/t_{FR,test}$
This paper	Square TRC	TRC-0.4-0	250	2.2	3.81	8ϕ16	0	280.7	40.8	441.33	1576	86.7	86.7	1.00
	Square TRC	TRC-0.5-0	250	2.2	3.81	8ϕ16	0	280.7	40.8	441.33	1957	38.1	38.1	1.00
	Square TRC	TRC-0.6-0	250	2.2	3.81	8ϕ16	0	280.7	40.8	441.33	2446	13.5	13.5	1.00
	Square TRC	TRC-0.5-25	250	2.2	3.81	8ϕ16	25	280.7	40.8	441.33	1343	45.5	45.5	1.00
	Square TRC	TRC-0.5-50	250	2.2	3.81	8ϕ16	50	280.7	40.8	441.33	1028	35.6	35.6	1.00
Ref. [42]	Circular TRC	STCRC-1	300	2.53	3.81	8ϕ20	0	291.3	58.6	357.4	1340	116.5	116.9	1.00
	Circular TRC	STCRC-2	300	2.53	3.81	8ϕ20	0	291.3	58.6	357.4	1800	82.5	90	1.09
	Circular TRC	STCRC-3	300	2.53	3.81	8ϕ20	0	291.3	58.6	357.4	2240	50	53.9	1.08
	Circular TRC	STCRC-4	300	2.53	3.81	8ϕ20	0	291.3	58.6	357.4	2240	53.5	53.9	1.01
Ref. [47]	Square CFST	SP-1	219	5.3	3.81	-	0	246	15	-	950	169	157	0.93
	Square CFST	SP-2	350	7.7	3.81	-	0	284	15	-	2700	140	144	1.03
	Square CFST	SP-3	350	7.7	3.81	-	52.5	284	15	-	1670	109	112.8	1.03
Ref. [48]	Square CFST	S1	150	8	3.18	4ϕ12	75	452.7	45	548	161.1	26	27.7	1.07
	Square CFST	S2	220	10	3.18	4ϕ16+4ϕ10	110	560.3	39.7	527(ϕ16) 575.3(ϕ10)	446.5	23	26.5	1.15
	Square CFST	S3	150	8	3.18	4ϕ12	0	452.7	43.2	548	404.3	32	28	0.88
	Square CFST	S4	220	10	3.18	4ϕ16+4ϕ10	0	560.3	42.4	527(ϕ16) 575.3(ϕ10)	882.9	54	41.7	0.77
	Square CFST	S5	150	8	3.18	8ϕ12	112.5	452.7	48.7	548	133.2	29	31.4	1.08
	Square CFST	S6	220	10	3.18	4ϕ20+4ϕ16	110	560.3	38.8	576(ϕ20) 527(ϕ16)	452.6	29	33.8	1.17
	Circular CFST	C1	193.7	8	3.18	6ϕ12	96.9	359.1	36.4	512.4	186.7	26	31.6	1.22
	Circular CFST	C2	273	10	3.18	6ϕ16	136.5	369.7	37.6	553.5	387.5	30	51.2	1.71
	Circular CFST	C3	193.7	8	3.18	6ϕ12	0	359.1	43.2	512.4	535.6	29	26.5	0.91

Table 5 (cont'd) Details of the fire tests of TRC and CFST columns

Reference	Column Type	Column No.	D (mm)	t_s (mm)	L (m)	Re-bars	e (mm)	f_y (MPa)	f_c' (MPa)	f_b (MPa)	N_f (kN)	$t_{FR,test}$ (min)	$t_{FR,FE}$ (min)	$t_{FR,FE}/t_{FR,test}$
Ref. [48]	Circular CFST	C4	273	10	3.18	6ϕ16	0	451.1	37.8	553.5	882.9	72	65.3	0.91
	Circular CFST	C5	193.7	8	3.18	6ϕ16	145.3	359.1	35.8	553.5	152.4	29	41	1.41
	Circular CFST	C6	273	10	3.18	8ϕ20	136.5	369.7	36.9	566.5	391.5	57	49.8	0.87
Ref. [50]	Circular CFST	C159-6-3-30-20-20	159	6	3.18	-	20	332	35.8	-	169	32	27.52	0.86
	Circular CFST	C159-6-3-30-20-40	159	6	3.18	-	20	332	42.2	-	337	16	21	1.31
	Circular CFST	C159-6-3-90-20-20	159	6	3.18	-	20	332	73.7	-	272	34	30.12	0.89
	Circular CFST	C159-6-3-90-20-40	159	6	3.18	-	20	342.6	74.6	-	544	11	14	1.27
	Circular CFST	C159-6-3-30-50-20	159	6	3.18	-	50	343.6	30.5	-	126.4	29	32.5	1.12
	Circular CFST	C159-6-3-30-50-40	159	6	3.18	-	50	365.7	38.3	-	252.8	23	19.55	0.85
	Circular CFST	C159-6-3-90-50-20	159	6	3.18	-	50	365.7	79.1	-	194	30	28.4	0.95
	Circular CFST	C159-6-3-90-50-40	159	6	3.18	-	50	365.7	98.3	-	388	16	18.5	1.16
	Circular CFST	RC159-6-3-30-20-20	159	6	3.18	4ϕ12	20	357.2	39	500	180	47	47.5	1.01
	Circular CFST	RC159-6-3-30-20-40	159	6	3.18	4ϕ12	20	357.2	40.4	500	360	24	23	0.96
	Circular CFST	RC159-6-3-90-20-20	159	6	3.18	4ϕ12	20	357.2	93.7	500	263.8	48	54	1.13
	Circular CFST	RC159-6-3-90-20-40	159	6	3.18	4ϕ12	20	386.4	96	500	527.7	22	22.8	1.04
	Circular CFST	RC159-6-3-30-50-20	159	6	3.18	4ϕ12	50	386.4	31	500	140	39	38	0.97
	Circular CFST	RC159-6-3-30-50-40	159	6	3.18	4ϕ12	50	386.4	39.5	500	279.9	20	21.6	1.08
	Circular CFST	RC159-6-3-90-50-20	159	6	3.18	4ϕ12	50	315.2	93	500	203.7	40	48	1.20
	Circular CFST	RC159-6-3-90-50-40	159	6	3.18	4ϕ12	50	315.2	91.9	500	407.4	15	18	1.20
Ref. [54]	Square CFST	SQ-1	152.4	6.35	3.81	-	0	350	58.3	-	376	66	67	1.02
	Square CFST	SQ-2	152.4	6.35	3.81	-	0	350	46.5	-	286	80	72.01	0.90
	Square CFST	SQ-7	177.8	6.35	3.81	-	0	350	57	-	549	86	84.5	0.98
	Square CFST	SQ-17	254	6.35	3.81	-	0	350	58.3	-	1096	62	65	1.05
	Square CFST	SQ-20	254	6.35	3.81	-	0	350	46.5	-	931	97	107.2	1.11
	Square CFST	SQ-24	304.8	6.35	3.81	-	0	350	58.8	-	1130	131	127	0.97

Table 5 (cont'd) Details of the fire tests of TRC and CFST columns

Reference	Column Type	Column No.	D (mm)	t_s (mm)	L (m)	Re-bars	e (mm)	f_y (MPa)	f_c' (MPa)	f_b (MPa)	N_f (kN)	$t_{FR,test}$ (min)	$t_{FR,FE}$ (min)	$t_{FR,FE}/t_{FR,test}$
Ref. [54]	Circular CFST	C-02	141.3	6.55	3.81	-	0	350	33.1	-	110	55	65.4	1.19
	Circular CFST	C-04	141.3	6.55	3.81	-	0	350	31	-	131	57	52.8	0.93
	Circular CFST	C-05	168.3	4.78	3.81	-	0	350	32.7	-	150	76	85.6	1.13
	Circular CFST	C-08	168.3	4.78	3.81	-	0	350	35.5	-	218	56	71.1	1.27
	Circular CFST	C-11	219.1	4.78	3.81	-	0	350	31	-	492	80	89.9	1.12
	Circular CFST	C-13	219.1	4.78	3.81	-	0	350	32.3	-	384	102	110.9	1.09
	Circular CFST	C-17	219.1	8.18	3.81	-	0	350	31.7	-	525	82	84.9	1.04
	Circular CFST	C-20	273.1	5.56	3.81	-	0	350	28.6	-	574	112	169.1	1.51
	Circular CFST	C-21	273.1	5.56	3.81	-	0	350	29	-	525	133	183.4	1.38
	Circular CFST	C-22	273.1	5.56	3.81	-	0	350	27.2	-	1000	70	84.7	1.21
	Circular CFST	C-23	273.1	12.7	3.81	-	0	350	27.4	-	525	143	169.8	1.19
	Circular CFST	C-25	323.9	6.35	3.81	-	0	350	27.6	-	699	145	159.8	1.10
	Circular CFST	C-26	323.9	6.35	3.81	-	0	350	24.3	-	1050	93	93.4	1.00
	Circular CFST	C-29	355.6	12.7	3.81	-	0	350	25.4	-	1050	170	236.2	1.39
	Circular CFST	C-31	141.3	6.55	3.81	-	0	300	30.2	-	80	82	74.8	0.91
	Circular CFST	C-32	141.3	6.55	3.81	-	0	300	34.8	-	143	64	50.6	0.79
	Circular CFST	C-34	219.1	4.78	3.81	-	0	300	35.4	-	500	111	94.9	0.85
	Circular CFST	C-35	219.1	4.78	3.81	-	0	300	42.7	-	560	108	99.6	0.92
	Circular CFST	C-37	219.1	8.18	3.81	-	0	300	28.7	-	560	102	72.4	0.71
	Circular CFST	C-40	273.1	6.35	3.81	-	0	300	46.5	-	1050	106	144.6	1.36
	Circular CFST	C-42	273.1	6.35	3.81	-	0	300	55.4	-	1050	90	110.9	1.23
	Circular CFST	C-44	273.1	6.35	3.81	-	0	300	38.7	-	715	178	175	0.98
	Circular CFST	C-45	273.1	6.35	3.81	-	0	300	38.2	-	712	144	173.4	1.20
	Circular CFST	C-50	323.9	6.35	3.81	-	0	300	42.4	-	820	234	317.2	1.36

Table 5 (cont'd) Details of the fire tests of TRC and CFST columns

Reference	Column Type	Column No.	D (mm)	t_s (mm)	L (m)	Re-bars	e (mm)	f_y (MPa)	f_c' (MPa)	f_b (MPa)	N_f (kN)	$t_{FR,test}$ (min)	$t_{FR,FE}$ (min)	$t_{FR,FE}/t_{FR,test}$
Ref. [55]	Square CFST	SQ-12	203.2	6.35	3.81	$4\phi16$	0	350	47	400	500	150	143.3	0.96
	Square CFST	SQ-13	203.2	6.35	3.81	$4\phi16$	0	350	47	400	930	105	89.92	0.86
	Square CFST	SQ-18	254	6.35	3.81	$4\phi19.5$	0	350	48.1	400	1440	113	112.5	1.00
	Square CFST	SQ-19	254	6.35	3.81	$4\phi19.5$	0	350	48.1	400	2200	70	82	1.17
	Square CFST	SQ-22	304.8	6.35	3.81	$4\phi16+4\phi19.5$	0	350	47	400	3400	39	35.94	0.92
	Square CFST	SQ-23	304.8	6.35	3.81	$4\phi25.2$	0	350	47	400	2000	212	215.3	1.02
	Circular CFST	C-48	273.1	6.35	3.81	$4\phi19.5$	0	350	46.7	400	1050	188	154	0.82
	Circular CFST	C-49	273.1	6.35	3.81	$4\phi19.5$	0	350	47	400	1900	96	88	0.92
Ref. [81]	Circular CFST	C1-1	478	8	3.81	-	0	293	31.7	-	4700	29	31.6	1.09
	Circular CFST	C1-2	478	8	3.81	-	71.7	293	31.7	-	2200	32	30.3	0.95
	Circular CFST	C2-1	219	5	3.81	-	32.9	293	31.7	-	450	17	12.9	0.76
	Circular CFST	C2-2	219	5	3.81	-	65.7	293	31.7	-	300	18	16.5	0.92
	Circular CFST	C2-3	219	5	3.81	-	0	293	31.7	-	960	132	93.8	0.71
	Circular CFST	C2-4	219	5	3.81	-	0	293	31.7	-	960	175	156.1	0.89
													Mean	1.05
													Std. dev.	0.18

Notes: "D" width of the square section or diameter of the circular section; "t_s" steel tube thickness; "L" whole column length; "ϕ" diameter of the reinforcing bar; "e" load eccentricity; "f_y" steel tube yield strength; "f_c'" concrete cylinder compressive strength; "f_b" reinforcing bar yield strength; "N_f" applied axial load in fire test; "$t_{FR,test}$" tested fire resistance; "$t_{FR,FE}$" FEA predicted fire resistance.